DATA SUPPLEMENTS

MATERIALS AND METHODS

Materials

ß-amidotaurocholate (BATC) was synthesized according to published methods (67). NBD-FA was from Molecular Probes Inc. (Eugene, OR, USA). Collagenase (Worthington, CLS type I, 190-250 units/mg) was provided by Biochrom (Berlin, Germany). Human recombinant insulin was supplied by the biotechnology department of Sanofi Pharma Germany (Frankfurt am Main, Germany). Partially purified phosphatidylinositol-specific phospholipase C (PI-PLC) from *Bacillus cereus* (1 unit/mg protein), phosphatidylcholine-specific phospholipase C (PC-PLC) from *Clostridium perfringens* (25 units/mg protein), phospholipase A_2 (PLA_2) from honey bee venom (*Apis mellifera*)(1800 units/mg), bovine serum albumin (BSA; fraction V, defatted), rat serum albumin (RSA), phenylisopropyladensine (PIA), adenosine deaminase (ADA), PMSF, purified α-mannosidase from *Canavalla ensiformis* (proteomics grade), saponin, digitonin, filipin, nystatin and cAMP-agarose were obtained from Sigma-Aldrich Chemie GmbH (Munich, Germany). Recombinant (*E. coli*) human glycosylphosphatidylinositol-specific phospholipase D1 (GPI-PLD1)(0.5 units/mg protein) was purchased from Creative BioMart Inc. (New York, USA). Streptolysin-O was bought from VWR Scientific. 5'-AMP-agarose was delivered by Jena Bioscience GmbH (Jena, Germany). Anti-CD73 antibodies (rabbit polyclonal, affinity-purified, IgG isotype, prepared against recombinant full-size human CD73 with reactivity against rat CD73) were obtained from Genetex/Biozol (Eching, Germany). Annexin-V (human, recombinant) was purchased from ProSpec (East Brunswick, NJ, USA). Recombinant (*E. coli*) *N*-glycanase F from *Flavobacterium meningosepticum*, recombinant (*Pichia pastoris*) proteinase K (PCR grade), protease inhibitor cocktail ("complete ULTRA" tablets), octylglucoside (OG) and Nonidet-P40 (NP-40) were provided by Roche Biochemicals (Mannheim, Germany). GF/C glass fiber filters were delivered by Whatman (Maidstone, UK). 5'-AMP-Sepharose beads were purchased from LKB/Pharmacia (Freiburg, Germany). "Stains-all" was provided by ICN Biochemicals (Cleveland, OH, USA). 1-ethyl-3-[3-dimethylaminopropyl]carbodiimide (EDC) and N-hydroxysulfosuccinimide (Sulfo-NHS, premium grade) were bought from Pierce/Thermo Scientific (Rockford, IL, USA). Tetrahydrofurane (THF), PBS (tablets), TRIS, HEPES, MES, silver nitrate, thin layer chromatography (TLC) plates (Si-60), dinonylphtalate, ethanolamine, mannose, Tween, glycine and all other reagents (highest purity available) were from Merck (Darmstadt, Germany).

Animal Handling

16 male Wistar rats (Crl:WI(WU)), 16 male Zucker diabetic fatty rats (ZDF-*Lepr^{fa}*/Crl) and 15 male Zucker fatty rats (Crl:ZUC(Orl)-*Lepr^{fa}*/Zucker)(68), respectively, were obtained from Charles River (Sulzfeld, Germany). The male ZDF rats were 14 weeks old at start of the induction of the lean and obese phenotype, respectively. At this age, male obese ZDF rats already exhibit a full-blown diabetic phenotype with a catabolic metabolic state. This explains the same body weight range of lean and obese ZDF rats at this age. Rats were housed two *per* cage in an environmentally controlled room with a 12:12-h light–dark circle (light on at 06:00) and *ad libitum* access to food and water. Standard rat chow (17.7 kJ/g, Ssniff diet R/M-H, V1535

with 18% crude protein, 4.7% sugar, and 3.5% crude fat) and a cafeteria diet (21.6 kJ/g, Ssniff diet EF R, 10 mm with 13.5% crude protein, 42.8% sugar, and 22.5% crude fat)(Ssniff, Soest, Germany) were used for the induction of the lean and obese phenotype, respectively, as described previously (69). All experimental procedures were conducted in accordance with the German Animal Protection Law (paragraph 6) and corresponded to international animal welfare legislation and rules.

Serum Collection

Blood was collected from the tail vein of conscious rats under terminal isoflurane, placed in serum gel tubes and centrifuged (1,000x*g*, 5 min, 4°C) to yield serum, which was immediately frozen in liquid N_2 and then stored at -20°C. The samples were thawed by incubation at 37°C and then immediately used for measurement unless indicated otherwise. Blood metabolic parameters were determined enzymatically according to standard procedures using commercially available kits (for glucose Gluco-quant glucose/HK kit; Roche, Mannheim, Germany) and the Hitachi 912 instrument. Insulin concentration was assayed for 15 µl of sample volume with an enzyme immunoassay (ultrasensitive rat insulin ELISA; Mercodia 10-1248-10, Uppsala, Sweden) covering a sensitivity range of 0.5-100 µg/l and displaying the following crossreactivities: Human insulin 167%, porcine insulin 476%, sheep insulin 179%, bovine insulin 78%. All assays were performed according to the instructions of the manufacturers.

Human serum was collected using standard clinical procedures. Glucose was measured with the aid of the Glucose HK Gen.3 kit (Roche Diagnostics, Mannheim, Germany). Written informed consent was obtained from all study participants, and the protocol was approved by the ethical review committee of the Ludwig-Maximilians-University.

Chemical Synthesis of Phosphoinositolglycans (PIG) and (G)PI-PLC Inhibitor GPI-2350

The methods for the synthesis of PIG41 and PIG37 have been described previously (47). In brief, the glycosidic linkages have been made stereoselective by the trichloroacetimidiate methodology. For introduction of the phosphate, the tetrabenzylpyrophosphate/sodium hydride or the phosphitylation/oxidation protocol was used. For introduction of the sulfate, a solution of trimethylamine-sulfur trioxide complex in pyridine was used. The structure of the PIG was characterized by mass, ^{1}H NMR und ^{31}P NMR spectroscopy. The method for the synthesis of GPI-2350 has been outlined in detail previously (59). In brief, racemic 1,4,5,6-tetra-*O*-benzyl-*myo*-inositol was phosphorylated with dodecyl-phosphonic dichloride in the presence of triethylamine and dimethyl-aminopyridine. The resulting tetra-*O*-benzyl-*myo*-inositol-1,2-cyclo-dodecyl-phosphonic acid was debenzylated by catalytic hydrogenation on charcoal to yield *myo*-inositol-1,2-cyclo-dodecyl-phosphonic acid (GPI-2350) as a mixture of diastereomeres.

Preparation of Isolated Rat Adipocytes

Isolated rat adipocytes were prepared as described previously (70) with the following modifications: Rats were killed by cervical dislocation. Epididymal fat pads from male Wistar rats (weight see below, fed ad libitum) were washed several times in Krebs-Ringer-Henseleit buffer (KRH; 25 mM HEPES free acid, 25 mM HEPES sodium salt, 1.2 mM KH_2PO_4, 140 mM NaCl, 4.7 mM KCl, 1.2 mM $MgSO_4$, 2.5 mM $CaCl_2$)

supplemented with 0.75% (w/v) BSA and adjusted to pH 7.2 (=KRHLB) and then cut into two to three pieces. Two pieces each were incubated with 1.5 ml of digestion buffer (10 mg collagenase and 9 mg glucose in 10 ml of KRH containing 5% BSA [=KRHHB], 1 mM sodium pyruvate, 5.5 mM glucose, 0.5 U/ml ADA, 200 nM PIA, 100 µg/ml gentamycin, 50 units/ml penicillin and 50 µg/ml streptomycin sulfate) for 15–20 min at 37°C in a shaking water bath (240 cycles/min) at constant bubbling with 95% O_2/5% CO_2. Released adipocytes were passed through a nylon web (mesh size 750 *µ*M) with no pressure other than gentle teasing with a plastic spatula for passing of the cells through and then centrifuged (500x*g*, 1 min, swing-out rotor). The supernatant layer of cells was washed three times with 25 ml each of KRH by centrifugation. After final aspiration of the infranatant, the adipocytes were suspended in KRH containing 2% BSA at a lipocrit of 10% corresponding to 100 µl of packed cell volume *per* ml incubation volume (determined by aspiration of small aliquots into capillary hematocrit tubes and centrifugation for 60 sec in a microhematocrit centrifuge in order to determine the fractional occupation of the suspension by the adipocytes). 10% lipocrit corresponds to about 6.5, 1.5 and $0.3x10^6$ adipocytes of small, medium and large size, respectively, *per* ml.

Size Separation of Adipocytes

Adipocytes were separated according to size using published procedures (71) with the following modifications: Adipocytes prepared from 1-month (120-140 g), 2-month (200-240 g) and 6-month (380-420 g) old male rats were collected by flotation (200x*g*, 2 min, 30°C) and then filtered through serial nylon mesh screens with pore sizes of 400, 150 and 75 µm in this order to obtain small adipocytes (diameter < 75 µm from 1-month old rats) from the flow-throughs or 75, 150 and 400 µm in this order to obtain large adipocytes (diameter > 400 µm) from the filter cakes or 400, 75 and 150 µm in this order to obtain middle-sized adipocytes (75 µm < diameter < 150 µm from 2-months old rats) from the flow-through, filter cake and flow-through, respectively. After fixation of aliquots of the adipocyte suspension with osmic acid, cell number was determined using a Coulter counter. The adipocyte suspension was adjusted to the desired titer with adipocyte buffer (20 mM HEPES/KOH, pH 7.4, 140 mM NaCl, 4.7 mM KCl, 2.5 mM $CaCl_2$, 1.2 mM $MgSO_4$ and 1.2 mM KH_2PO_4,) supplemented with 0.5% BSA, 100 µg/ml gentamycin, 50 units/ml penicillin and 50 µg/ml streptomycin sulfate. Total lipid content of the adipocyte suspension (lipocrit) was measured as described above.

Measurement of Insulin Sensitivity and Responsiveness of Adipocytes as Insulin-stimulated Lipogenesis

Adipocytes were assayed for lipogenesis as described previously (70) with the following modifications: 200 *µ*l of adipocyte suspension were supplemented with 190 *µ*l of KRHLB containing 1 mM glucose and 10 *µ*l of an insulin solution to yield the desired final concentration and incubated (15 min, 37°C) in a slowly shaking water bath. The assay was started by addition of 50 *µ*l (unless otherwise indicated) of 0.9 mM NBD-FA (prepared daily from a 100-mM stock solution in ethanol by dilution with KRHLB under mild heating). After incubation (90 min, 37°C) under mild shaking (stage 11, thermomixer, Eppendorff, Germany), lipogenesis was terminated by filtration of the total mixtures over GF/C-filters under vacuum. The filters were rapidly washed three times with 1 ml of KRHLB each, placed in 20-ml plastic scintillation vials and extracted with 400 *µ*l THF for 15 min under rigorous shaking. 300 *µ*l of the extract was transferred into new tubes and centrifuged (15,000x*g*, 5 min). The supernatant was dried (SpeedVac) and suspended in 50 *µ*l THF. 5-*µ*l

samples were analysed by TLC on silica gel Si-60 plates using 78 ml diethyl ether, 22 ml petrol ether and 1 ml acetic acid as solvent system. The amount of fluorescent lipid products on the dried plates was determined by fluorescence imaging with excitation at 460 nm and emission at 540–560 nm using a phosphorimaging system. The relative peak area of each lipid product were corrected for a background value (derived from an equal-sized region of the TLC plate which does not contain any lipid product).

Preparation of Plasma Membranes from Rat Adipocytes

Plasma membranes were prepared from primary rat adipocytes as described previously (71) with the following modifications: Adipocytes (10^7 cells) prepared from epididymal adipose tissue depots were washed and immediately homogenized in 2 ml of lysis buffer (25 mM TRIS/HCl, pH 7.4, 0.5 mM EDTA, 0.25 mM EGTA and 0.25 M sucrose, supplemented with 10 g/ml leupeptin, 2 µM pepstatin, 10 g/ml aprotinin, 5 µM antipain and 200 µM PMSF) using a motor-driven Teflon-in-glass homogenizer (10 strokes with a loosely fitting pestle) at 22°C. The defatted postnuclear infranatant (1,500x*g*, 5 min) was centrifuged (12,000x*g*, 15 min). The pellet was suspended in 1 ml of lysis buffer and layered on top of an 8-ml cushion of 28% Percoll, 0.25 M sucrose, 25 mM TRIS/HCl (pH 7.0) and 1 mM EDTA. After centrifugation (45,000x*g*, 60 min), the purified plasma membranes were withdrawn from the lower third of the gradient (0.5 ml), then pelleted (200,000x*g*, 90 min) and finally suspended in 10 mM HEPES/KOH (pH 7.5), 150 mM NaCl and 100 mM sucrose at 50 µg protein/ml.

Preparation of Incubation Medium from Rat Adipocytes

Adipocytes were suspended in 10 ml of adipocyte buffer (20 mM HEPES/KOH, pH 7.4, 140 mM NaCl, 4.7 mM KCl, 2.5 mM $CaCl_2$, 1.2 mM $MgSO_4$, 1.2 mM KH_2PO_4, 2% (w/v) BSA, 100 µg/ml gentamycin, 1 mM sodium pyruvate and 5.5 mM glucose) at a lipocrit of 0.2% and then incubated (20 h, 37°) in a shaking water bath (100 cycles/min) under constant bubbling with 5% CO_2/95% O_2. Thereafter, twelve 350-µl portions of the total mixtures were transferred into microfuge tubes (Beckman) pre-filled with 100 µl of dinonylphtalate and then centrifuged (1,000x*g*, 1 min, 20°C). The tubes were cut through the dinonylphtalate layer separating the adipocytes at the top from the incubation medium in the bottom part of the tubes which was rescued. Care was taken to minimize the volume of dinonylphtalate taken along with the incubation medium in the bottom part. After transfer of the incubation medium (300 µl) into 1-ml Eppendorf cups and washing the bottom part of the tube once with 300 µl of adipocyte buffer containing 0.5 mM DTT and protease inhibitor mix, the combined medium and washing fluid were centrifuged (1,000x*g*, 5 min, 4°C) for the removal of cell debris.

Preparation of Total and Gce1-/CD73-Harboring EV from Rat Adipocytes

EV from isolated rat adipocytes were obtained using published procedures (71) with the following modifications: For preparation of total EV, three 180-µl portions of the supernatant obtained were centrifuged (Beckman Airfuge, A-110 fixed angle rotor, 30 psig, 110,000 rpm, 30 min, 4°C). After careful aspiration of the supernatants, the pellets were resuspended in 100 µl of EV buffer (10 mM TRIS/HCl, pH 7.4, 250 mM sucrose, 1 mM EDTA, 0.5 mM EGTA, 140 mM NaCl, 1 mM DTT and protease inhibitor cocktail) each

(vortexing), combined and re-centrifuged as above. The pellet was washed two times with 100 µl each of the same buffer. After purification by sucrose density gradient centrifugation (200,000x*g*, 18 h, Beckman SW41) on 10-70% sucrose in PBS prepared with Gradient Mate device (BioComp, Fredericton, New Brunswick, Canada), fractions with densities of 1.12-1.22 mg/ml were combined, diluted ten-fold with PBS and centrifuged (100,000x*g*, 2 h, 4°C). The pelleted total EV were suspended in the initial volume of EV buffer and re-centrifuged.

For affinity purification of Gce1- and CD73-harbouring EV, total EV were adsorbed to cAMP-agarose and 5'-AMP-Sepharose, respectively. For this, 100-µl suspensions were supplemented with 200 µl of cAMP-agarose/5'-AMP-Sepharose beads (50 mg each in 1 ml of 100 mM HEPES/KOH, pH 7.4, 140 mM NaCl, 1 mM $MgCl_2$, 0.5 mM DTT and protease inhibitor cocktail) and then incubated under continuous head-over rotation (60 cycles *per* min) of the tubes. Thereafter, the incubation mixtures were centrifuged under conditions (1,000x*g*, 5 min, 4°C), which did not lead to sedimentation of unadsorbed EV (lacking Gce1 and CD73) *per se*, but were sufficient for the quantitative sedimentation of the Sepharose beads (with the Gce1-/CD73-harbouring EV adsorbed). The collected bead-EV complexes were washed twice by suspending in 1 ml of EV buffer, each, and centrifugation (1,000x*g*, 5 min, 4°C). The final pellet was dissociated in 100 µl of EV buffer containing 100 µM AMP and cAMP each. After incubation (30 min, 4°C) and centrifugation (12,000x*g*, 5 min, 4°C), the supernatant containing the Gce1-/CD73-harbouring EV was recovered, frozen in liquid N_2 and stored at -80°C until use.

Enzymatic Pretreatment of Samples

Lipases. 20 µl of serum or 4.5 ml of incubation medium were supplemented with 80 µl of 1x PI-PLC buffer (20 mM TRIS/HCl, pH 7.8, containing 0.1% BSA, 144 mM NaCl, 0.5 mM EDTA, 1 mM DTT and 0.1 mM PMSF), PLA_2 buffer (25 mM HEPES/KOH, pH 7.2, containing 0.1% BSA, 144 mM NaCl, 2 mM Ca^{2+}, 1 mM DTT and 0.1 mM PMSF) or PC-PLC buffer (20 mM TRIS/HCl, pH 7.8, containing 0.1% BSA, 144 mM NaCl, 2 mM Zn^{2+}, 1 mM DTT and 0.1 mM PMSF) or GPI-PLD buffer (10 mM TRIS/maleate, pH 7.4, containing 144 mM NaCl, 1 mM Ca^{2+}, 1 mM DTT and 0.1 mM PMSF) or 500 µl of the corresponding 10x buffers, respectively, and then incubated (30 min, 30°C) with partially purified PI-PLC from *Bacillus cereus* as described previously (72) or PLA_2 from honey bee venom or PC-PLC from *Chlostridium perfringens* (73) or recombinant human GPI-PLD, respectively, at the concentrations indicated in the figure legends.

Proteinase K. 50 µl of serum were supplemented with 200 µl of PBS and then incubated (60 min, 4°C) with proteinase K at the concentrations indicated in the absence or presence of 1 mM PMSF.

N-Glycanase F. 50 µl of serum were supplemented with 200 µl of 0.1 M sodium phosphate buffer (pH 8.6), 1 mM DTT and 0.1 mM PMSF and then incubated (30 min, 30°C) with *N*-glycanase F from *Flavobacterium meningosepticum* at the concentrations indicated in the absence or presence of 0.5 M sodium thiocyanate.

α-Mannosidase. 50 µl of serum were supplemented with 200 µl of 25 mM TRIS/HCl (pH 7.5) and 30 mM NaCl and then incubated (30 min, 30°C) with α-mannosidase from *Canavalla ensiformis* at the concentrations indicated in the absence or presence of 10 mM $HgCl_2$.

Chemical Pretreatment of Samples

Pretreatments for the chemical degradation of GPI structures were performed as described previously (73-76) with the following modifications:

Dephosphorylation by hydrogen fluoride (HF). 50 µl of serum were supplemented with 200 µl of 50% (w/v) HF (T) or NaCl (C) and 0.5 M pyridine at -20°C in a polyethylene tube fitted with a cap. After incubation (60 min, 0 $\pm$ 0.5°C), the mixture was poured into a stirred saturated solution of LiOH at 4°C and then rapidly adjusted to pH 7.0 by the dropwise addition of 1 M LiOH. Prior to measurement, HF was removed under a stream of N_2.

Deamination by nitrous acid (NA). 50 µl of serum were supplemented with 200 µl of 60 mM sodium acetate buffer (pH 4.0) containing 333 mM $NaNO_3$ and then incubated (60 min, 22°C) as adapted from a previous report (74).

Immunoblotting

Proteins separated by sodium polyacrylamide gel electrophoresis (SDS-PAGE) were transferred to polyvinylidene difluoride membranes using the semi-dry procedure as described previously (46). Washed membranes were incubated (24 h, 4°C) with anti-CD73 antibodies (1:1500), again washed and then incubated (3 h, 4°C) with horseradish peroxidase-coupled secondary goat anti-mouse IgG antibodies (1:4000). Labeled proteins were visualized by enhanced chemiluminescence. Lumiimages were evaluated with a luminescence imager using LumiImager software (Roche Diagnostics).

Silver Staining and Densitometry

A protocol for “Stains-all“ was used modified for enhanced sensitivity as described previously (77). After SDS-PAGE (Novex precast gels, 10% acrylamide, BIS/TRIS resolving gel, morpholinopropanesulfonic acid-SDS running buffer), the gel was incubated (30 min) ten times with 100 ml of 25% isopropanol, each, on a shaker. Thereafter, the gel was incubated (25°C, 4-6 h) with 50 ml of “Stains-all“ solution (30 mM TRIS/HCl, pH 8.7, 7.5% formamide, 25% isopropanol containing 0.025% [w/v] “Stains-all“) in light-tight containers on an orbital shaker. Subsequently, the gel was washed three times with 50 ml of 25% isopropanol, each, with a change every 10 min until the background became clear, then rinsed five times with water and finally incubated (40 min) in 50 ml of 12 mM silver nitrate on an orbital shaker. After rinsing of the gel with water and then with developer solution (0.28 M sodium carbonate and 0.15% formaldehyde) three times for 30 sec, each, the gel was incubated (5-10 min) with developer solution until the protein bands were visible. After termination of the developing reaction by removal of developer and the addition of 10% acetic acid, the gel was stored in a solution of 5% glycerol and 10% acetic acid. Densitometric scanning was performed using the Gel Print System (BioPhotonic Corp.) with the Video Copy Processor P4OU (Mitsubishi Inc.). Quantitative evaluation was performed utilizing the software package GPTools v3.0, 1-D Gel Analysis Software (BioPhotonic Corp.).

Miscellaneous

Protein concentration was determined using the bicinchoninic acid protein assay kit (Thermo Fisher Scientific, Waltham, USA) with BSA as calibration standard.

SUPPLEMENTAL FIGURES S1-S18

Supplemental Figure S1. Coupling of α-toxin to the chip.

Rationale: Specific capture of unprocessed GPI-AP by the SAW chip-based sensor is accomplished by the protein α-toxin upon covalent coupling to the chip surface. GPI-AP act as receptors for bacterial cyto- and hemolytic toxins (78), such as α-toxin of the Gram-positive bacterium *Clostridium septicum* (79-81). Ample evidence is available that the highly conserved glycan core of the GPI anchor is the major binding determinant for α-toxin (4, 82-84) and that the diacylglycerol moiety of the GPI anchor, the *N*-glycans or the (carboxy-terminal) protein moiety of the GPI-AP play minor roles, only (85-88). Nevertheless, it can not be excluded at present that GPI anchors of different GPI-AP may differ in their relative affinity for α-toxin to a limited extent, which could be due to structural variation of the protein moiety of the GPI-AP.

Legend: Covalent coupling of α-toxin to the gold surface of long-chain 3D CM-dextran sam® 5 chips in comparison to the control molecules, MPP1 and RSA, was performed using a conventional EDC/NHS-based protocol and monitored by measuring the kinetics of the phase shift in course of the reaction. Following activation of free carboxyl groups of the CM-dextran chip surface in a SamX instrument with 200 µl EDC/NHS at a flow rate of 50 µl/min at 25°C (period A), erythrocyte membrane palmitoylated protein 1 (MPP1, turquoise curve, period B), rat serum albumin (RSA, red curve, period C) and *Clostridium septicum* α-toxin (green curve, period D), diluted to 150, 450 and 300 nM, respectively, were consecutively linked to the chip at 2x120-µl portions, each, at a flow rate of 60 µl/min using carboxylamide coupling (see Methods). Capping with 150 µl of 1 M ethanolamine ($EtNH_2$, pH 8.5) at a flow rate of 45 µl/min was performed in parallel in all channels (period E). As a control, the phase shift generated by an activated (by EDC/NHS) and capped (by $EtNH_2$) "blank" channel in course of injection of immobilization buffer lacking protein (black line) was recorded. Phase shift is given (as °) upon normalization (set at 0 for 0 sec). Green and black arrows indicate start and termination, respectively, of the solution flow. Representative diagram from three independent coupling reactions is shown for each condition with distinct channels of four chips.

(S1)

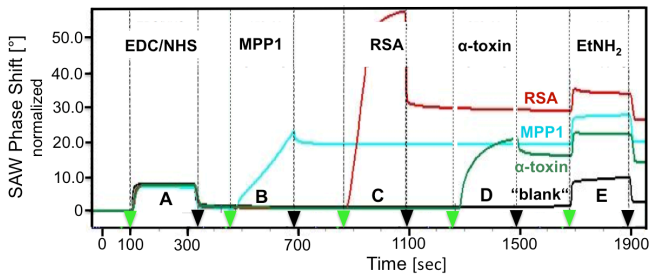

Outcome: The phase shifts elicited by covalent coupling of proteins (colored curves) to the chip surface compared to injection of the "blank" control (black curve) were similar for the three proteins with RSA (red curve) being most efficient under the experimental conditions used, followed by MPP1 (turquoise curve) and α-toxin (green curve).

Conclusion: α-toxin can be covalently coupled to the chips with considerable efficacy. The phase shifts generated by the sensor and recorded in real-time reflect the loading of mass onto the chip surface and, in addition, depend on the (bio-)physical properties of the contacting sample fluid, including and predominantly its viscoelasticity. Therefore, in the following experiments phase shifts and amplitudes were corrected for

unspecific effects caused by the sample fluid and non-GPI-mediated (i.e. unspecific) interaction of sample components with the chip by subtraction of the "blank" channel values measured upon sample injection.

Supplemental Figure S2. Effect of PIG41 on chip-based sensing of EV.

Rationale: To demonstrate the specificity of capture of GPI-AP equipped with the complete GPI anchor by the sensor, synthetic PIG, which more or less closely resemble the structure of the glycan core of the GPI anchor of mammalian GPI-AP and differ from one another in total length, side chains and linkages (47), were assayed for their capability to interfere with capture of EV or to induce their displacement from the chip.

Legend: 150 µl of EV in EV buffer or EV buffer alone ("control" and "blank" curves, only) were injected together with 400 nM annexin-V in the presence of 40 µM Ca^{2+} (period A) into α-toxin-coated channels of the chip ("control", yellow, green, red and grey curves) or into "blank" channels (brown and black curves) at a flow rate of 65 µl/min, followed by injection of 200 µl of EV buffer as running buffer (period B). Thereafter, 90 µl of PIG41 (yellow, 200 µM; grey, 100 µM; green, 30 µM; red, 10 µM) in EV buffer or EV buffer alone ("control") were injected at a flow rate of 20 µl/min (period C). After washing with 150 µl of EV buffer at a flow rate of 60 µl/min (period D) and subsequently with 150 µl at a flow rate of 90 µl/min (period E), 150 µl of EV in EV buffer containing 400 nM annexin-V and 40 µM Ca^{2+} in the presence or absence of the corresponding concentration of PIG41 in EV buffer were injected at a flow rate of 25 µl/min (period F). Phase shift is given (as °) upon normalization (set at 0 for 0 sec). Representative diagram from two independent coupling reactions is shown for each condition with distinct channels of four chips.

(S2)

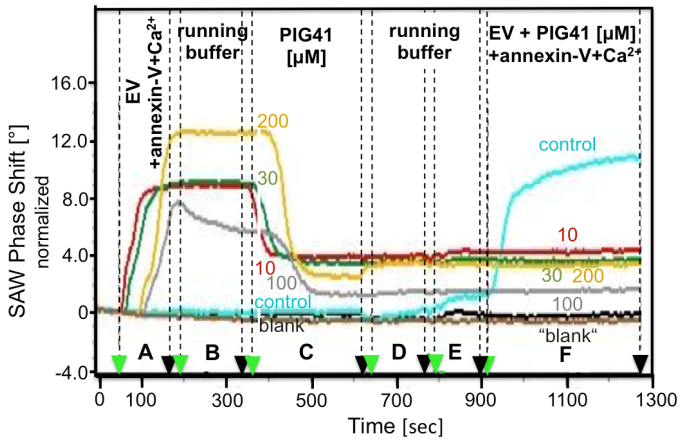

Outcome: Phase shifts were observed with the α-toxin-coated rather than with the "blank" channels which were maintained during washing indicating specificity of capture rather than mere adsorption of the EV and annexin-V to the chips (periods A and B). The phase shifts were considerably diminished upon injection of PIG41 in concentration-dependent fashion (period C). Following washing (periods D and E), injection of EV and annexin-V in the presence of corresponding concentrations of PIG41 did not result in increases in phase shift (period F). In contrast, in the absence of PIG41 injection of EV and annexin-V caused elevation of phase shift in the control channel, but not in the "blank" channel.

Conclusion: The phase shift observed with α-toxin-coated channels seems to rely on the capture of EV through specific interaction between the GPI anchor glycan core and the α-toxin and subsequent phospholipid detection by annexin-V binding, which can be modulated by synthetic PIG.

Supplemental Figure S3. Chip-based sensing of unprocessed GPI-AP in adipocyte incubation medium.

Rationale: Next, total incubation medium from primary rat adipocytes, which contains EV at rather low concentration only (5-7), was used to test the sensitivity and the potential for differentiation of the GPI-AP-harboring EV according to size and insulin sensitivity of the donor cells. The adipocytes considerably differed in their responsiveness and sensitivity towards insulin for the stimulation of lipogenesis and glucose transport with small adipocytes exhibiting the highest fold-stimulation above basal and the lowest EC_{50} compared to cells of medium and large size (Supplemental Table S1).

Legend: 2x150 µl of medium derived from the incubation of adipocytes of small, medium and large size at identical lipocrit or of medium alone ("medium" channel) were injected into α-toxin-coated channels at a flow rate of 25 µl/min. Subsequently, 2x150 µl of 20 mM TRIS/HCl (pH 8.0), 150 mM NaCl and 250 mM sucrose containing 400 nM annexin-V and 40 µM Ca^{2+} were injected at a flow rate of 25 µl/min (period A), followed by injection of 300 µl of 20 mM TRIS/HCl (pH 8.0), 150 mM NaCl, 2 mM EGTA containing 0.05% NP-40 at a flow rate of 180 µl/min (period B). Phase shift is given (as °) upon correction for the "blank" and "medium" channels and normalization (set at 0 for 0 sec and each size). Representative diagram from three independent coupling reactions is shown for each condition with distinct channels of six chips.

(S3)

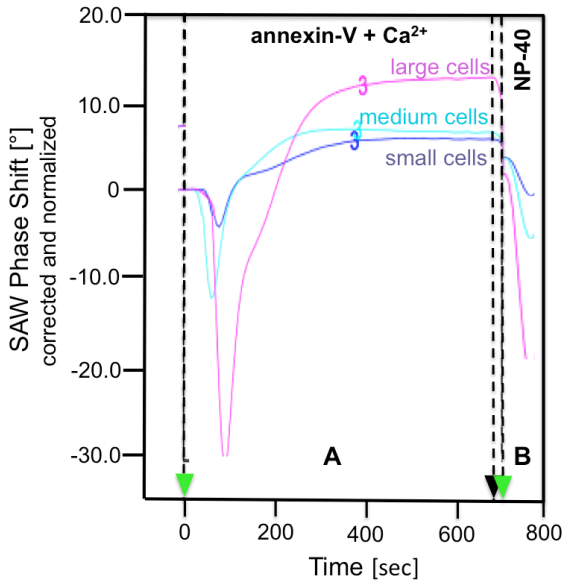

Outcome: Moderate differences in the time-resolved changes in phase shift after GPI-AP capture and phospholipid detection between crude incubation media from adipocytes of small, medium and large size were observed. Medium from large adipocytes caused the most prominent phase shifts, followed by media from adipocytes of medium and then small size. Injection of the detergent NP-40 caused drastic decline of the phase shift. This can not be explained by altered viscosity of the running buffer containing NP-40 *per se* (data not shown), but is most likely due to disintegration of the structure of the complexes containing unprocessed GPI-AP and lipids.

Supplemental Figure S4. Differential chip-based sensing of unprocessed GPI-AP in medium.

Rationale: The differentiating effect of synthetic PIG on the capture of unprocessed GPI-AP released from small, medium and large adipocytes was studied.

Legend (*A*): 2x150 µl of medium derived from incubation of adipocytes of small, medium and large size at identical lipocrit or of medium alone ("medium" channel) were injected into α-toxin-coated channels at a flow rate of 90 µl/min (period A). Subsequently, 2x150 µl of 20 mM TRIS/HCl (pH 8.0), 150 mM NaCl and 250 mM sucrose containing 10 µM PIG37 (left panel) or 200 µM PIG37 (right panel) were injected at a flow rate of 23 µl/min (period B). Phase shift is given (as °) upon correction for the "blank" and "medium" channel and normalization (set at 0 for 0 sec and each adipocyte size). Representative diagrams from two independent capture processes are shown for each condition with distinct channels of five chips.

(S4*A*)

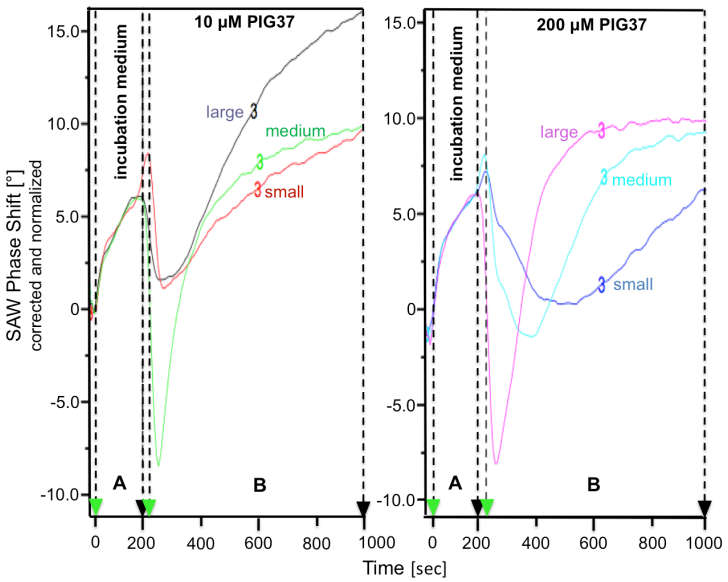

Outcome (*A*): The time-dependent increases in the phase shift following the injection of incubation medium (periods A) were considerably and differentially affected by the presence of 10 and 200 µM PIG37 (periods B) with moderate and pronounced interference with the capture, respectively. 10 µM PIG37 is sufficient for small and medium adipocytes, whereas 200 µM is required for large adipocytes. Thus, PIG37 modulates the capture of unprocessed GPI-AP released from adipocytes by the α-toxin-coated chip, which seems to rely on structural characteristics of the GPI-AP in complex with lipids, which apparently differ between medium from adipocytes of small, medium and large size.

Legend (*B*): 2x150 µl of incubation medium from adipocytes of small, medium and large size at identical lipocrit or of medium alone ("medium" channel) were injected into α-toxin-coated channels (period A1/2) at a flow rate of 90 µl/min. Subsequently, 300 µl of 20 mM TRIS/HCl (pH 8.0), 150 mM NaCl and 250 mM sucrose containing 30 µM PIG37 (period B1/2) and then 2x200 µl of the same buffer containing 200 µM PIG41 (period C1/2) were injected at a flow rate of 30 µl/min. Phase shift is given (as °) upon correction for the "blank" and "medium" channels and normalization (set at 0 for start of the injections and each adipocyte size). Representative diagrams are shown from two independent detection reactions with two distinct chips each using the same samples.

(4*B*)

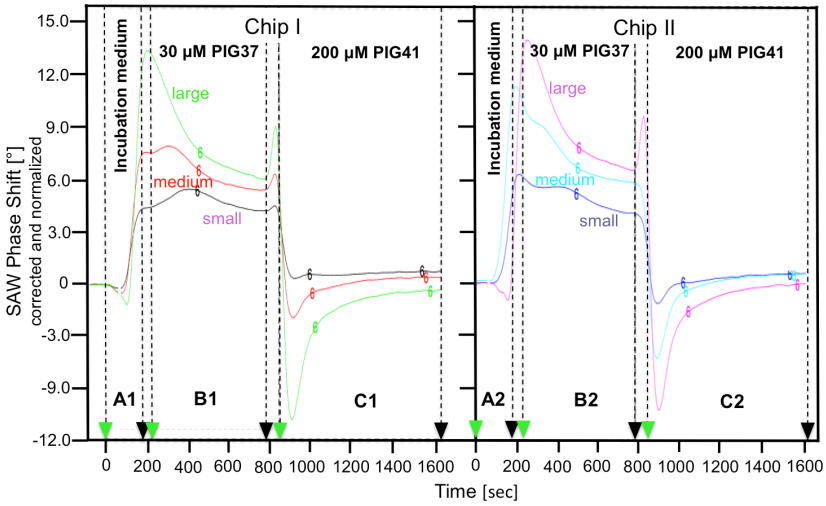

Outcome (*B*): Following injection of PIG37 at 30 µM during capture of unprocessed GPI-AP contained in the incubation medium with the accompanying increases in phase shift for adipocytes of large, medium and small size in that declining ranking order (period A1/2), the phase shift decreased in time-dependent fashion with incubation medium from large adipocytes being affected most pronouncedly (period B1/2). Complete elimination of the medium-induced phase shift was provoked upon injection of PIG41 at 200 µM (period C1/2), which was independent of the size of the adipocytes. The experiment was performed with two distinct chips (Chip I and II), independently coated with α-toxin, to demonstrate the high reproducibility of the PIG37-modulated capture and PIG41-induced displacement. Importantly, the kinetics of both capture and displacing of the medium GPI-AP were modulated by PIG37 and PIG41 in differential and reproducible fashion.
Conclusion (*B*): The presence of 30 µM PIG37 and 200 µM PIG41 during capture and for displacement, respectively, favors the differentiation of unprocessed GPI-AP of diverse nature/origin as shown here for those released from adipocytes of different size.

Legend (*C*): 75 µl of medium derived upon incubation of adipocytes of small (red curves), medium (blue curves) and large (grey curves) size at identical lipocrit or of medium alone ("medium" channel) and 75 µl of 20 mM TRIS/HCl (pH 8.0), 150 mM NaCl, 250 mM sucrose, 80 µM Ca^{2+} and 800 nM annexin-V were injected into the channels 1-4 of chip I (for the incubation without PIG37) and channels 5-8 of chip II (for the incubation with PIG37) at a flow rate of 90 µl/min (period A1/2). Thereafter, 125 µl of 20 mM TRIS/HCl (pH 8.0), 150 mM NaCl and 250 mM sucrose containing 30 µM PIG37 or lacking PIG37 was injected at a flow rate of 30 µl/min (period B1/2), followed by injection of 100 µl of 20 mM TRIS/HCl (pH 8.0), 150 mM NaCl and 250 mM sucrose at a flow rate of 150 µl/min (period C1/2). For displacement of the GPI-AP, 120 µl of 20 mM TRIS/HCl (pH 8.0), 150 mM NaCl and 250 mM sucrose containing 200 µM PIG41 or lacking PIG41 was injected at a flow rate of 20 µl/min (period D1/2). Amplitude is given (as arb. units) after correction for the "blank" and "medium" channels and normalization (set at 1 for 0 sec and large adipocytes). Representative diagrams from two independent capture/detection reactions are shown for each condition with 12 channels of three chips (re-used four times).

(4*C*)

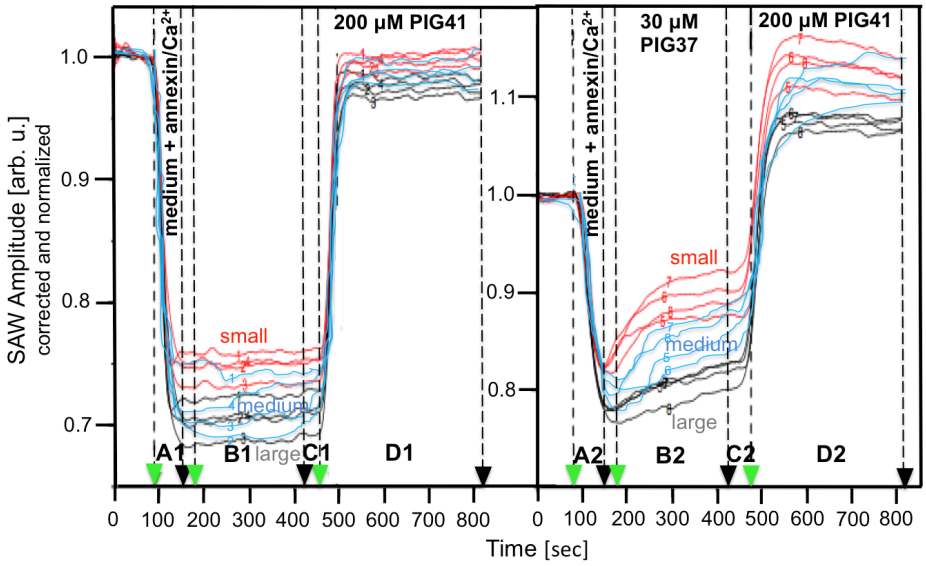

Outcome (*C*): The amplitude was drastically reduced upon simultaneous injection of the unprocessed GPI-AP and annexin-V with medium from large adipocytes being most effective, followed by medium-sized and small cells (periods A1/2). The presence of 30 µM PIG37 during capture led to differential declines of the amplitude reductions, i.e. to differential amplitude increases (periods B2), compared to the absence of PIG37 (periods B1), which followed the same ranking order. Upon injection of 200 µM PIG41, the amplitudes rapidly increased independent of the absence or presence of PIG37 during the previous capture/detection, reflecting the release of the captured GPI-AP. Furthermore, the comparison of injection of identical samples into the four channels of the same chip in parallel (identical colors) exemplified the high reproducibility of the chip-based sensing of unprocessed GPI-AP in incubation medium.

Supplemental Figure S5. SDS-PAGE/immunoblotting analysis of GPI-AP in adipocyte incubation medium.

Rationale: Changes in the amount of total or specific released GPI-AP were analyzed by one-dimensional SDS-PAGE (and immunoblotting) with or without prior enrichment of GPI-AP, since this could represent a rapid, convenient and cheap alternative for the chip-based sensing. The enrichment with magnetic microspheres coupled to α-toxin was aimed to circumvent the putative problem of masking of subtle differences in the amount of low-abundance GPI-AP in the total incubation medium by the majority of typical secretory proteins of adipocytes.

Legend: 10 ml of incubation medium, derived from incubation of adipocytes of small (green curves), medium (blue curves) and large (red curves) size at identical lipocrit, were left untreated (*A*, total proteins) or added to magnetic microspheres coupled to α-toxin (*B*, enriched GPI-AP). After magnetic separation (60 sec, see Methods), the washed microspheres were suspended in 100 µl of 2-fold Laemmli buffer by vortexing, sonication (20 sec) and heating (95°C, 5 min) in the dark. The supernatants were removed and transferred into new tubes. After the first extraction of the microspheres, this procedure was repeated. The supernatants of the first and second extraction were removed and combined (*B*). 80 µl of the untreated samples were supplemented with 20 µl of 5-fold Laemmli buffer, then heated (95°C, 5 min) and finally centrifuged (10,000x*g*, 2 min)(*A*). 20-µl portions of the supernatant samples were resolved by SDS-PAGE with four portions of each incubation medium applied to the left half and another four portions applied to the right half,

separated by two lanes with molecular weight markers (BluRAY Prestained Protein Ladder, Genedirex Inc.). The gels for the total (*A*) and enriched (*B*) samples were cut into two halves, each. One half was subjected to silver staining, the other half was cut into halves again, which were then used for immunoblotting of CD73 and Gce1. The gels were scanned for optical density. Samples from four distinct incubations with adipocytes of the three sizes, each, were analyzed by four gels. The corresponding curves represent the means of the major peaks, which were identified unambiguously between the gels, with SD given for their peak heights (as thin lines). The positions of CD73 (70 kDa) and Gce1 (59 kDa) are indicated.

(S5*A*)

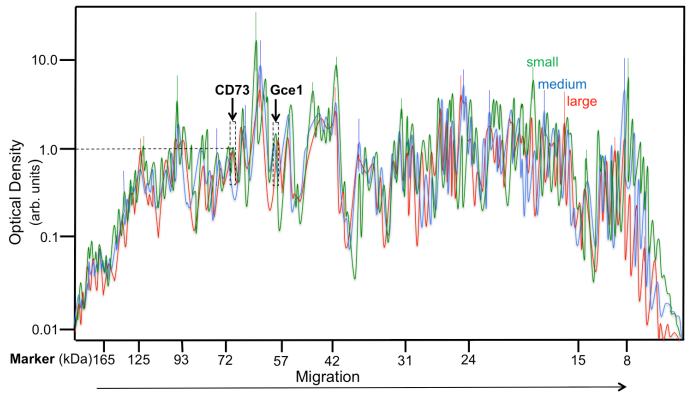

(S5*B*)

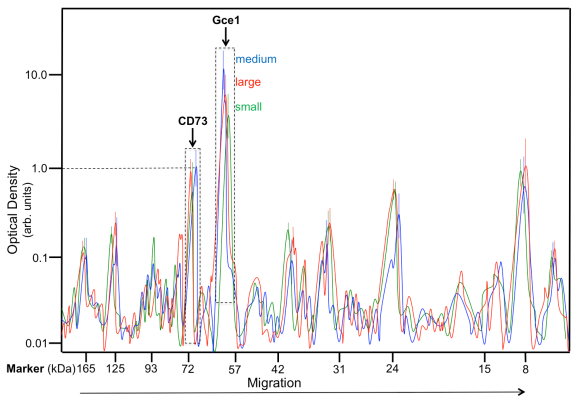

Outcome: The analysis of the total patterns of proteins released from primary rat adipocytes into the incubation medium by SDS-PAGE and subsequent silverstaining demonstrated the complexity of the adipocyte secretome as has been amply documented in the past (89-91). As expected, within the resolving power of the one-dimensional SDS-PAGE and silverstaining, the secretome did not reveal marked differences in the patterns of the total polypeptides between adipocytes of small, medium or large size (*A*). Immunoblotting for the two GPI-AP, CD73 and Gce1, led to their unambiguous identification in the unfractionated incubation medium, which is compatible with the previously demonstrated expression of CD73 and Gce1 in EV released from primary rat adipocytes (92). Interestingly, the amounts of CD73 and Gce1 in the unfractionated medium did not differ significantly between adipocytes of different size (*A*). In course of the fractionation procedure, which enables enrichment of GPI-AP harboring the intact as well as the lipolytically cleaved GPI anchor (4), a number of GPI-AP were found to be released into the incubation medium, among them CD73 and Gce1 as the predominant species (*B*). In general, the patterns of released GPI-AP looked very similar between adipocytes of small, medium and large size and, in particular, the amounts of individual GPI-AP, including CD73 and Gce1, did not vary with the adipocyte size.

Conclusion: The failure to detect differences in the released GPI-AP (as manifested in their total pattern as well as with specific candidates) between adipocytes of small, medium or large size as revealed by chip-based sensing of unprocessed GPI-AP may be explained as follows: (i) The major portion of the identified GPI-AP, including CD73 and Gce1, is released from the plasma membranes of rat adipocytes by either constitutive or regulated lipolytic cleavage (93) and masks the minor portion of unprocessed GPI-AP, which is released in correlation to cell size, only. (ii) The differences in phase shift and amplitude as monitored for unprocessed GPI-AP from adipocytes of different size are not due to differences in the amount of GPI-AP released. Rather they rely on differences in spec. mass, size and biophysical properties (shape, buoyant density, viscoelasticity), which are determined by the relative abundance of GPI-AP, phospholipids (and

possibly other constituents) and their configuration in the complex. Those differences can be elucidated only by time-resolved capture/detection under the control of PIG37, but escape detection by mere analysis of the amount of (total or specific) GPI-AP.

Supplemental Figure S6. Extrinsic factors affecting the generation of unprocessed GPI-AP from plasma membranes.

Rationale: The role of extrinsic factors which may determine the efficacy of the release of unprocessed GPI-AP *in vitro* was studied.

Legend: The experiment was performed with plasma membranes from small adipocytes (see Fig. 3) using running buffer containing 0.05 mU/ml human GPI-PLD (black curves), 1.0 mU/ml PLA_2 from honey bee venom, 0.01% BSA, 144 mM NaCl, 2 mM Ca^{2+}, 1 mM DTT and 0.1 mM PMSF (grey curves), 5.0 mU/ml PC-PLC from *Chlostridium perfringens*, 0.01% BSA, 144 mM NaCl, 2 mM Zn^{2+}, 1 mM DTT and 0.1 mM PMSF (turquoise curves), 0.05% BATC and 144 mM NaCl (pink curves), 1.0% BATC and 144 mM NaCl (brown curves), 0.2% BSA and 144 mM NaCl (green curves) or 25 µg/ml nystatin and 144 mM NaCl (red curves) at a flow rate of 50 µl/min during period B (3000-6600 sec) and as controls running buffer alone at a flow rate of 50 µl/min (yellow curves) or 200 µl/min (blue curves). In the midst of period B (4800 sec) the buffer flow was stopped for 2 h and the chip kept at 30°C while remaining placed in the instrument. Phase shift (*A*, as °) and amplitude (*B*, as arbitrary units) measured during period D are given upon correction by subtracting the values of the "blank" channel and normalization (set at 0 and 1, respectively, for 7200 sec). Representative overlay diagrams from three independent experiments (periods A-D, D shown only) with distinct chips are shown performed with the same samples.

(S6*A*) **(S6*B*)**

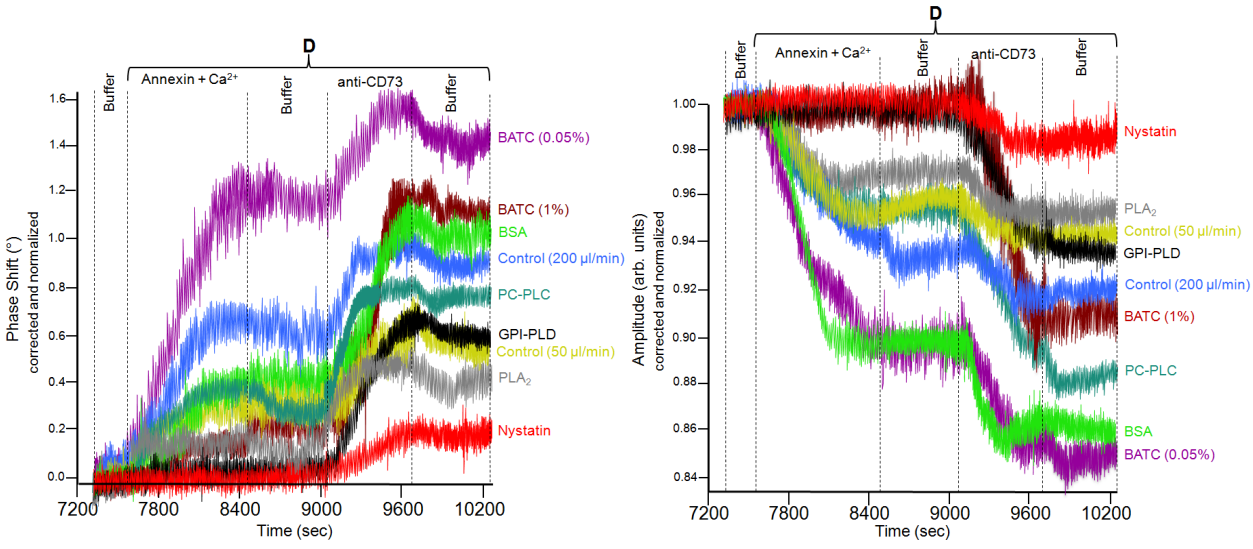

Outcome: Injection (at 50 µl/min flow rate) over a prolonged period of time with the detergent BATC at low concentration (pink curves), BSA (green curves) or PC-PLC (turquoise curves) led to considerable increases of phase shift (*A*) and decreases of amplitude (*B*) induced by sequential binding of annexin-V and, more pronounced, anti-CD73 antibodies compared to control (yellow curves) with BATC and BSA even exceeding the control injection at high flow rate (blue curves). BATC at high concentration (brown curves) and GPI-PLD (black curves) blocked the phase shift increase and amplitude reduction in response to annexin-V. In

contrast, BATC stimulated and GPI-PLD left unaffected the anti-CD73 antibody response compared to control. PLA_2 (grey curves) and nystatin (red curves) caused profound decrease and complete abrogation, respectively, of annexin-V-induced phase shift increase and amplitude reduction. In contrast, PLA_2 left unaltered and nystatin moderately impaired the anti-CD73 antibody-induced effects compared to control.
Conclusions: BATC at low concentration manages to selectively extract CD73 together with phospholipids from the plasma membranes, which result in mixed micellar structures and may resemble unprocessed GPI-AP released into the buffer stream. At high concentration BATC causes complete solubilization of CD73 into detergent micelles lacking phospholipids and cholesterol, which are clearly distinct from unprocessed GPI-AP. The fatty acid-binding BSA and the PC-PLC seem to stimulate the generation of unprocessed CD73 in complex with phospholipids, presumably through direct extraction from and phospholipid degradation within the plasma membranes, respectively. The latter is compatible with the cleavage specificity of the PC-PLC which does not encompass the GPI anchor (93) and apparently phospholipids when complexed to unprocessed GPI-AP. In contrast, GPI-PLD and PLA_2 activities cause removal of the phospholipids from the GPI anchor, which result in anchorless CD73 with the protein moiety left intact and captured *via* the glycan core of the GPI anchor. Finally, the cholesterol-sequestering compound nystatin drastically impairs the generation or/and structural integrity of the unprocessed GPI-AP and leaves small amounts of phospholipid-free CD73 protein moiety with the glycan core attached. This hints to the potential of cholesterol in the control of release or/and structure of complexes between unprocessed GPI-AP and lipids. However, it remains open whether the various treatments of the "lab-on-the-chip" are directed against the immobilized plasma membranes or the newly generated and captured GPI-AP.

Supplemental Figure S7. Implementation of chip-based sensing of unprocessed GPI-AP in rat serum.
Legend (*A*): Activated channels of a long-chain 3D CM-dextran sam®5 chip were coated (period A) with α-toxin (green curve) or left uncoupled as a "blank" channel (red curve), rinsed with running buffer (period B) and then capped by injection of 2x150 µl of 1 M ethanolamine ($EtNH_2$, pH 8.5) at a flow rate of 25 µl/min (period C). After rinsing with 2x100 µl of running buffer at a flow rate of 30 µl/min (period D), 40 µl of pooled serum sample from lean Wistar rats diluted five-fold with PBS or 200 µl PBS was injected into the coated (green curve) or "blank" (red curve) channel as indicated at a flow rate of 70 µl/min (periods E and F). Thereafter, 80 µl of 400 nM annexin-V in PBS containing 40 µM Ca^{2+} (period G), 70 µl of running buffer (period H), 80 µl of 200 nM anti-CD73 antibodies in PBS (period I) and finally running buffer (period K) were injected consecutively into the two channels at a flow rate of 120 µl/min. Phase shift was measured at 22°C and is given (in °) after normalization (set at 0 for start of the injections) as original data. Representative diagram from four independent coupling reactions is shown performed with channels of two chips (re-used two times).

(S7*A*)

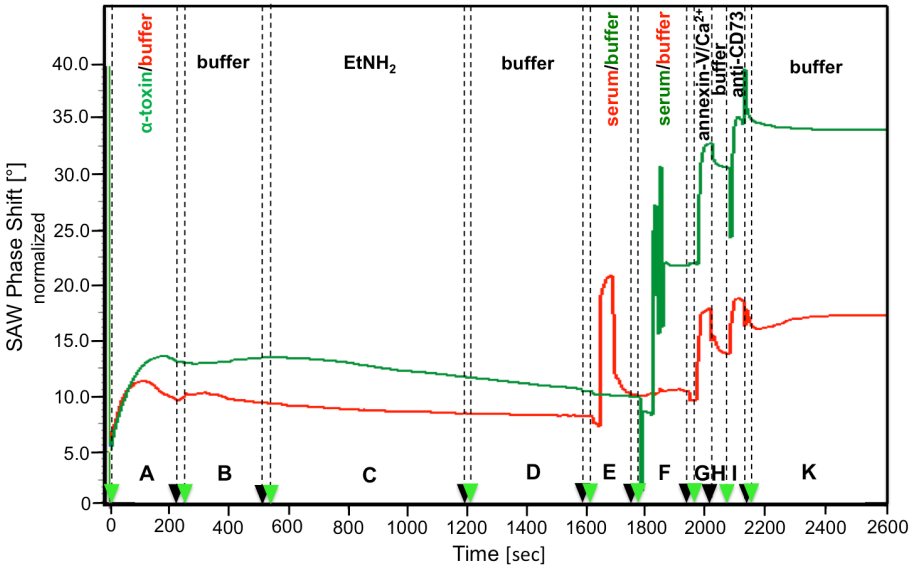

Outcome (*A*): The considerably increased and stably maintained phase shift measured upon coupling (period A) and subsequent consecutive washing (period B), capping (period C) and washing (period D), respectively, was further upregulated in course of successive injections of serum samples (periods E and F), annexin-V (period G) and anti-CD73 antibodies (period I). The stable elevations, as manifested by intermediary (period H) and final rinsing (period K) of the channels, were significantly higher for the α-toxin-coated channel compared to the "blank" channel.

Conclusion (*A*): Serum from Wistar rats apparently contains unprocessed GPI-AP which can be monitored on basis of capture by the chips and binding of annexin-V. The pronounced "background" signal elicited by serum in the "blank" channel may be due to the high abundance of albumin, which interacts with the chip surface by unspecific adsorption. In turn, the adsorbed albumin could capture phospholipids and unprocessed GPI-AP in serum *via* its fatty acid-binding sites. To correct for albumin-mediated annexin-V-induced phase shifts or amplitude reductions in the following experiments with serum-containing samples, "albumin" channels, coated with α-toxin and rinsed with RSA, and “blank” channels were run in parallel and the values subtracted from those measured for serum samples with α-toxin-coated channels.

Legend (*B*): 40 µl of pooled serum samples from lean Wistar (turquoise curve) and obese ZDF (black curve) rats, diluted five-fold with PBS, were injected into α-toxin-coated chips at a flow rate of 48 µl/min (period A). Following injection of 4x150 µl of PBS at a flow rate of 160 µl/min (period B), 2x125 µl of 400 nM annexin-V in PBS containing 40 µM Ca^{2+} were injected at a flow rate of 60 µl/min (period C). Following injection of 4x137.5 µl of PBS at a flow rate of 120 µl/min (period D), 50 µl of 10 ng/ml anti-CD73 antibodies in PBS were injected at a flow rate of 13 µl/min (period E). Phase shift is given (as °) after correction for the "blank" and "albumin" channels and normalization (set at 0 for start of the injections and 0 sec). Representative diagram from two independent capture/detection reactions for each condition is shown performed with channels of two chips.

(S7*B*)

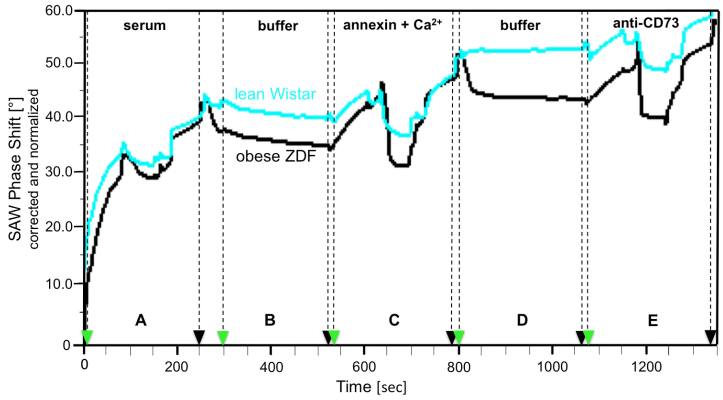

Outcome (*B*): Obese ZDF rats exhibited the highest fasting plasma glucose among the six animal groups tested reflecting their diabetic state and the differences in metabolic disturbances were apparently most pronounced between those and lean Wistar rats (Supplemental Table S2). However, measurement of the phase shift and amplitude (data not shown) did not reveal significant differences in the kinetics and maximal extent of capture of GPI-AP (period A) and subsequent detection of phospholipids by annexin-V (period C) and CD73 by anti-CD73 antibodies (period E) binding. The missing or only moderate reduction in maximal phase shift upon rinsing (periods B, D) hint to the stability of the capture and detection assemblies constituted by the serum GPI-AP, chip and detection molecules.

Legend (*C*): 40 µl of pooled serum samples from lean Wistar (turquoise curve) and obese ZDF (black curve) rats, diluted five-fold with PBS were injected into α-toxin-coated chips at a flow rate of 160 µl/min (period A). Thereafter, additional 40 µl of serum diluted five-fold with PBS and containing 30 µM PIG37 were injected at a flow rate of 120 µl/min (period B), followed by injection of 2x150 µl of 400 nM annexin-V in PBS containing 40 µM Ca^{2+} at a flow rate of 36 µl/min (period C). Subsequently, 4x150 µl of running buffer were injected at a flow rate of 75 µl/min (period D). Phase shift is given (as °) after correction for the "blank" and "albumin" channels and normalization (set at 0 for start of the injections and 0 sec). Representative diagram from three independent capture/detection reactions for each condition is shown performed with channels of three chips.

(S7*C*)

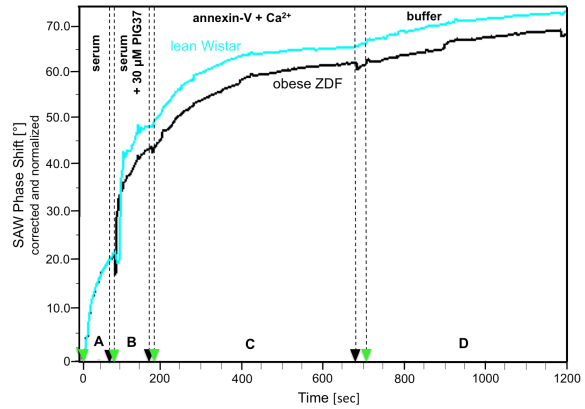

Outcome (*C*): A consistent difference between obese ZDF and lean Wistar rats was observed with the latter displaying a more rapid and pronounced increase in stable (during rinsing; period D) phase shift in course of

capture in the presence of PIG37 (period B) and subsequent phospholipid detection by annexin-V (period C). In contrast, in the absence of PIG37 the phase shift increases measured for the two serum samples were almost identical (period A).

Legend (*D*): 40 µl of pooled serum samples from lean Wistar (turquoise curve) and obese ZF (black curve) rats, diluted five-fold with PBS were injected into α-toxin-coated chips at a flow rate of 120 µl/min (period A). Thereafter, additional 40 µl of serum diluted five-fold with PBS and containing 30 µM PIG37 were injected at a flow rate of 160 µl/min (period B), followed by injection of 2x150 µl of 400 nM annexin-V in PBS containing 40 µM Ca^{2+} at a flow rate of 35 µl/min (period C). Subsequently, 4x150 µl of running buffer were injected at a flow rate of 90 µl/min (period D). Phase shift is given (as °) after correction for the "blank" and "albumin" channels and normalization (set at 0 for start of the injections and 0 sec). Representative diagram from two independent capture/detection reactions for each condition is shown performed with channels of two chips.

(S7*D*)

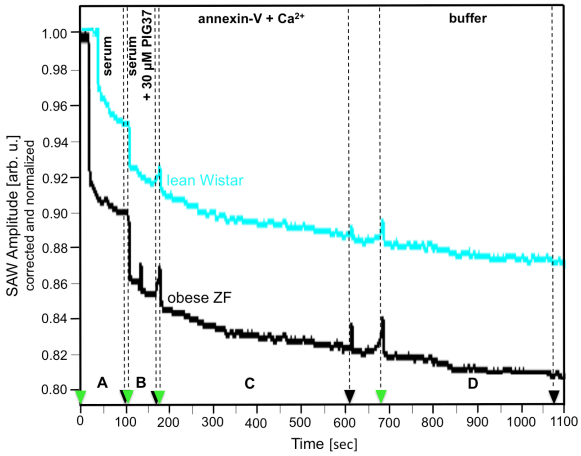

Outcome (*D*): At variance with the phase shift increase, the kinetics of capture as reflected in the amplitude reduction revealed more drastic differences between sera of metabolically differing rats, exemplified by lean Wistar and obese ZF rats. The serum of the latter animals, which exhibited a pronounced hyperinsulinemia and normoglycemia due to their insulin-resistant non-diabetic state (Supplemental Table S2), elicited a faster and more pronounced reduction in amplitude even during the initial absence of PIG37 (period A), which became further upregulated in course of presence of 30 µM PIG37 (period B) as well as annexin-V (period C). This PIG-dependent difference persisted during the final rinsing (period D).

Conclusion (*D*): The presence of 30 µM PIG37 at the midst of the capture, enables the differentiation between lean Wistar and lean ZDF or obese ZF rats by monitoring the phase shift and amplitude, respectively.

Legend (*E*): 40 µl of pooled serum samples from obese Wistar (green curve) and lean ZF (red curve) rats, diluted five-fold with PBS were injected into α-toxin-coated chips at a flow rate of 250 µl/min (period A1). Thereafter, 75 µl of 400 nM annexin-V in PBS containing 40 µM Ca^{2+} were injected at a flow rate of 30 µl/min (period B1). Subsequently, 150 µl of 200 µM PIG41 in PBS were injected at a flow rate of 120 µl/min (period C1). This cycle of GPI-AP capture (period A2-A4), phospholipid detection (period B2-4) and GPI-AP displacment (period C2-4) was repeated three times with increasing concentrations of PIG37 during capture

as indicated. Final regeneration of the chip was accomplished by injection of 300 µl PBS containing 0.05% NP-40 at a flow rate of 120 µl/min (period D). Amplitude is given (as arb. units) after correction for the "blank" channel and "albumin" channel (injection of RSA without/with NP-40) and normalization (set at 1 for start of the injections A1 and 0 sec). Representative diagram from six independent capture/detection reactions for each condition is shown performed with channels of three chips (re-used two times) using the same samples.

(S7*E*)

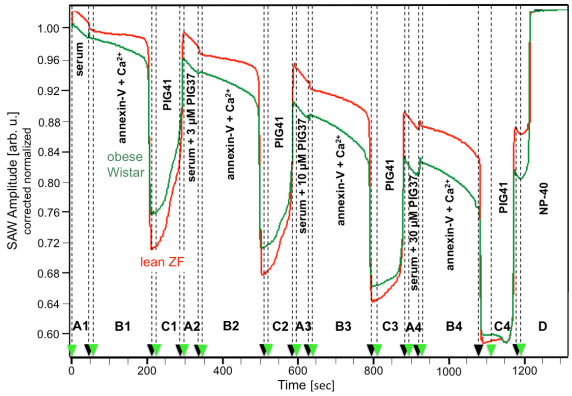

Legend (*F*): 40 µl of pooled serum samples from obese Wistar (green curve) and lean ZDF (red curve) rats, diluted five-fold with PBS were injected into α-toxin-coated chips at a flow rate of 75 µl/min (period A1). Thereafter, 50 µl of 400 nM annexin-V in PBS containing 40 µM Ca^{2+} was injected at a flow rate of 60 µl/min (period B1). Subsequently, 25 µl of 200 µM PIG41 in PBS was injected at a flow rate of 15 µl/min (period C1). This cycle of GPI-AP capture (A2-A4), phospholipid detection (period B2-4) and GPI-AP displacment (C2-4) was repeated three times with increasing concentrations of PIG37 during capture as indicated. Phase shift is shown (as arb. units) after correction for the "blank" channel and "albumin" channel (injection of RSA without/with NP-40, period D not shown) and normalization (set at 1 for start of the injections A1 and 0 sec). Representative diagram from four independent capture/detection reactions for each condition is shown performed with three distinct chips (re-used two times) using the same samples.

(S7*F*)

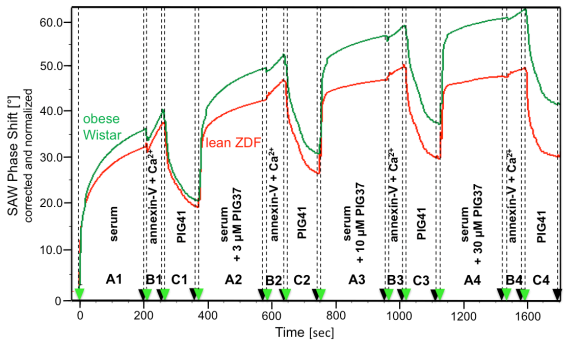

Outcome (*E, F*): Measurement of the time-resolved increases in amplitude reduction and phase shift revealed that the differences between obese Wistar and lean ZF/ZDF rats became gradually more pronounced with increasing concentrations of PIG37 (after correction for the considerable downward shift of the base line for 1.00 and 0, respectively, due to incomplete displacement by PIG41). Both amplitude and phase shift were rapidly and completely restored upon injection of NP-40. Apparently, the unprocessed GPI-

AP became detached from the α-toxin-coated chip as well as from annexin-V upon detergent solubilization compatible with their lipidic nature. Obese Wistar rats exhibited moderate hyperinsulinemia as a consequence of obesity-induced insulin resistance, whereas both lean ZDF and lean ZF rats did not have elevated fasting insulin levels compared to lean Wistar rats (Supplemental Table S2), making their differentiation on basis of chip-based sensing more demanding.

Conclusion (*E, F*): The inclusion of PIG37 after initiation of the capture is prerequisite for the differentation of obese Wistar *vs*. lean Z(D)F rats, but not for the reciprocal comparison of metabolic "extremes", i.e. healthy lean Wistar *vs*. diabetic obese Z(D)F rats.

Legend (*G*): 40 µl of pooled serum sample from lean Wistar rats diluted five-fold with PBS were injected into α-toxin-coated chips at a flow rate of 50 µl/min (periods A). Thereafter, 2x90 µl of 400 nM annexin-V in PBS containing 40 µM Ca^{2+} were injected at a flow rate of 25 µl/min (periods B). Displacement of the GPI-AP was initiated by injection of 50 µl of 200 µM PIG41 in PBS at a flow rate of 25 µl/min (periods C1), followed by injection of 2x150 µl of PBS containing 2 mM EGTA and 0.05% NP-40 at a flow rate of 100 µl/min (periods D1). After regeneration of the channels with 2x125 µl of PBS at a flow rate of 120 µl/min (periods E1), 40 µl of pooled serum sample from lean Wistar rats, diluted five-fold with PBS and incubated (10 min, 22°C) in the presence of 40 µM Ca^{2+} and 400 nM annexin-V, was injected at a flow rate of 25 µl/min (periods AB). The following periods C2, D2 and E2 were performed as described for the initial cycle. Phase shift (upper panel) and amplitude (lower half) are given (as ° and arb. units, respectively) after correction for the "blank" channel and "albumin" channel (injection of RSA without/with NP-40) and normalization (set at 0° and 1 arb. unit, respectively, for start of the injection A and 0 sec). Representative diagram from 8 independent experiments is shown performed with channels of two chips (re-used four times).

(S7*G*)

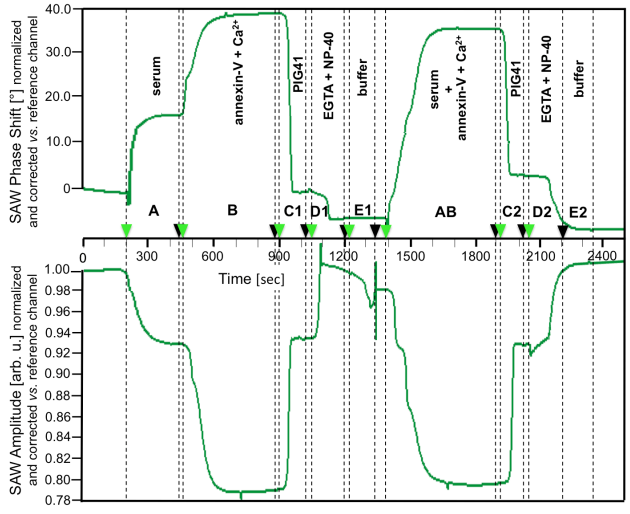

Outcome (*G*): The comparison between the sequential (periods A, B) and combined (periods AB) GPI-AP capture and phospholipid detection steps displayed no significant differences in the maximal phase shift increase as well as amplitude reduction. Displacement of the GPI-AP from the chip by PIG41 was less efficient for the combined protocol (periods C2). However, complete regeneration of the chips was accomplished using the combination of EGTA and NP-40 (periods D2) as indicated by the return to basal values for both phase shift and amplitude. This simplified protocol with simultaneous injection of serum

samples and annexin-V was used for the comparisons between rats of identical genotype and different body weight as well as between rats of similar body weight and different genotype.

Supplemental Figure S8. Evaluation of optimal serum volume and chip variance.

Legend (*A*):

The experiments for evaluation of the optimal sample volume were performed with increasing volumes of pooled serum samples from eight obese Wistar, ZF and ZDF rats each, diluted five-fold with PBS (total injection volume kept constant at 250 µl with PBS). The differences in maximal phase shift or minimal amplitude between the indicated rat groups were measured at the end of period AB (see Supplemental Fig. 7*G*) and are given as means ± SD from four to eight independent experiments performed with channels of two to four chips (re-used four times) using the same samples. * $p \leq 0.05$ and $^{\#}p \leq 0.01$ *vs*. PBS set at 0.

(S8*A*)

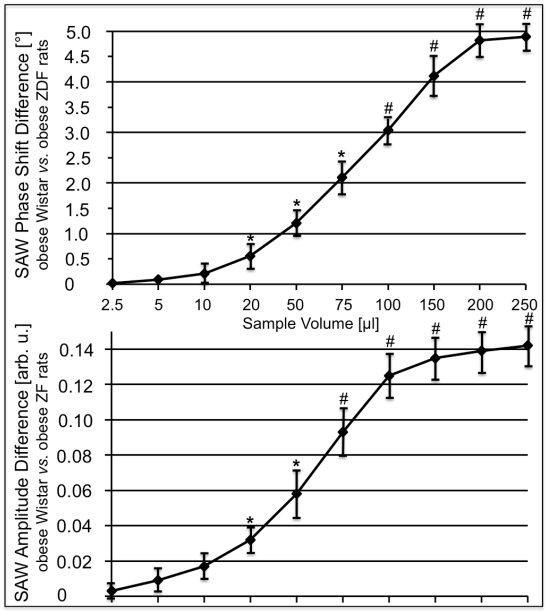

Outcome (*A*): Injection of sample volumes of 20 µl to up to 250 µl after dilution, corresponding to 4 to 50 µl rat serum resulted in significant differences in the maximal phase shift between obese Wistar and ZDF rats and in the minimal amplitude between obese Wistar and ZF rats. The most pronounced difference was obtained with 200 µl sample volume (corresponding to 40 µl serum) for serum from normal *vs*. insulin-resistant or diabetic rats. Thus the injection of up to 40 µl serum volume seems to be compatible with monitoring of putative differences in spec. mass, size, amount and viscoelasticity between unprocessed GPI-AP contained in rat serum samples.

Legend (*B*): The experiments for evaluation of the variance between chips and channels were performed with pooled serum samples from eight obese Wistar, ZF and ZDF rats each or PBS using the same channel after regeneration for three, six and nine cycles of capture/detection and displacement using two, three and four distinct channels of the same chip or two, four and six distinct chips using a single channel each. The differences in maximal phase shift and minimal amplitude measured at the end of period AB are given for

obese Wistar and ZDF rats (upper panel) as well as obese Wistar and ZF rats (lower panel), respectively, as means ± SD. * $p \leq 0.05$ and # $p \leq 0.01$ *vs*. the lowest number.

(S8*B*)

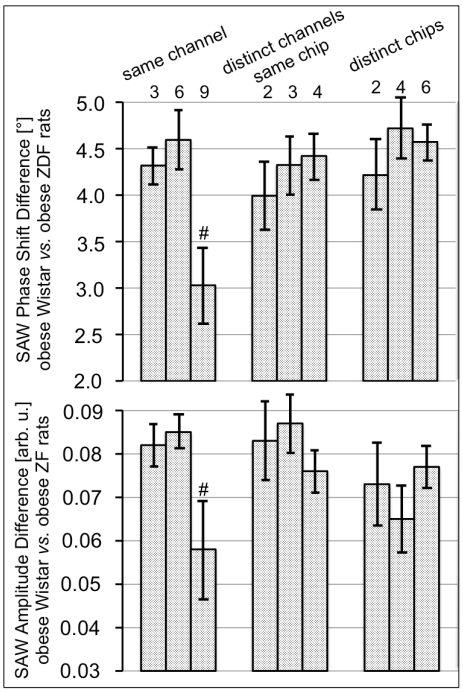

Outcome (*B*): Evaluation of the phase shift and amplitude differences between obese Wistar and obese Z(D)F rats revealed moderate non-significant deviations between three to six cycles of capture/detection, displacement and regeneration with the same channel, between two to four distinct channels of the same chip and between the channels of two to up to six distinct chips. However, after nine cycles of regeneration of the same channel, both phase shift and amplitude differences became significantly reduced with accompanying increases in variance, which is presumably due to gradual loss from the channel and/or reduced functionality of α-toxin and/or general impairment of the quality of the gold chip surface.

Conclusions (*A, B*): The following measurements with rat serum samples were routinely performed with 40 µl each and up to six cycles of capture/detection, displacement and regeneration using the same channel. Each serum sample was measured in two/three channels of the same chip resulting in 12/18 measurements. The remaining channels run on the same chip in parallel were used as "blank" and "albumin" channels (12/6/6 setting) or as "albumin" channel, only (18/6 setting).

Supplemental Figure S9. Differentiation of sera according to the genotype of the rats (ZF *vs*. ZDF) by chip-based sensing.

Legend: The experiments were performed (see Fig. 5) with sera from eight lean ZF and ZDF rats. Calculated means (M) ± SD for the individual samples or measured means for the pooled samples (P) ± SD are given performed with two chips for each rat group (18/6 setting).

(S9)

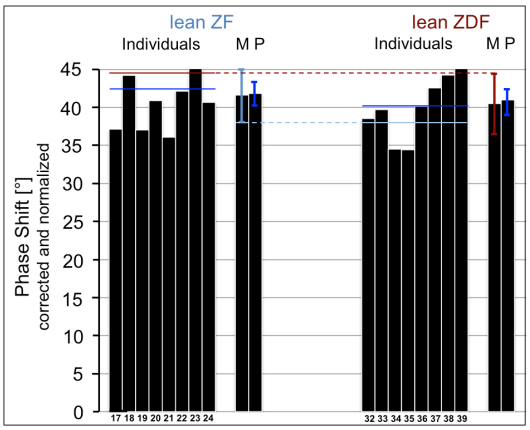

Outcome: Neither phase shift nor amplitude (data not shown) revealed significant differences or trends between lean ZDF and ZF rats with regard to the pooled serum samples (P) as well as the calculated means (M). Consequently, it was not possible to apply threshold values for the differentiation of individual rats with regard to their genotype. In conclusion, pairwise comparative measurement of the phase shift and amplitude enables the differentiation between individual lean Wistar and ZF or ZDF, respectively, rats, but not between lean ZF and ZDF rats.

Supplemental Figure S10. Differentiation of sera according to the body weight of the rats.

Legend: The minimal amplitudes (*A, B*) and maximal phase shifts (*C*) are calculated (see Fig. 4*C-H*) and given for the individual sera from eight lean and obese Wistar (*A*), lean and obese ZF (*B*) or lean and obese ZDF (*C*) rats.

(S10*A*)

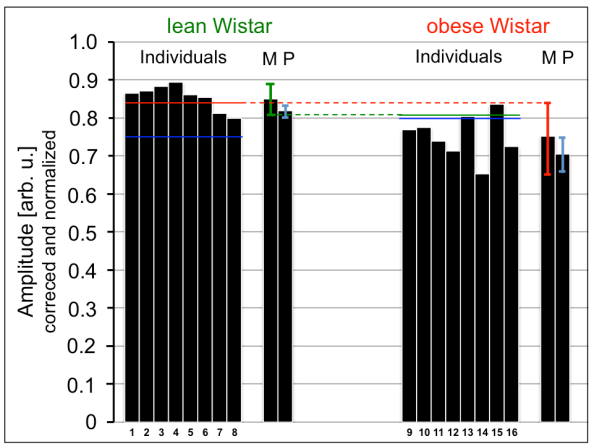

(S10*B*)

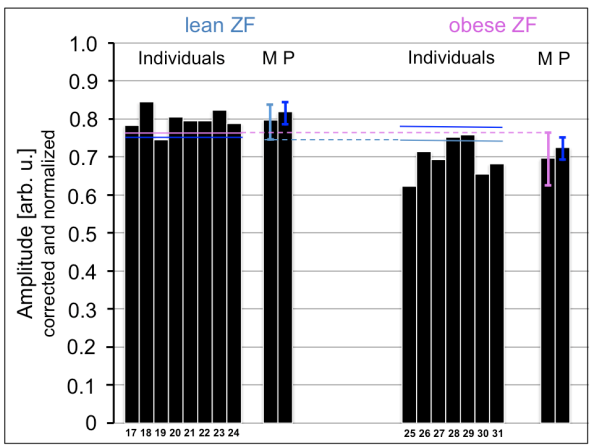

(S10*C*)

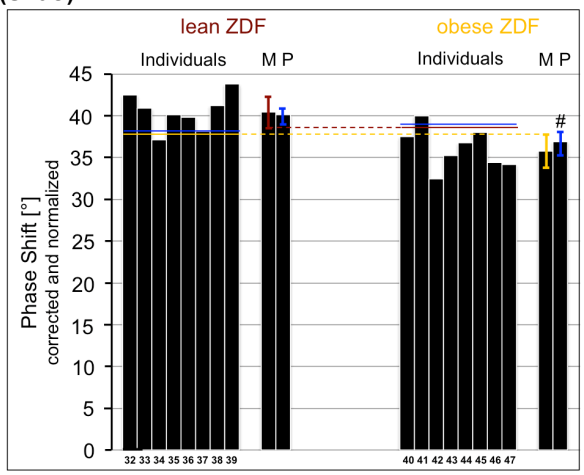

Outcome: Phase shift and amplitude measured for the pooled serum samples (P) as well as for the means calculated from the individual samples (M) of Wistar (*A*), ZF (*B*) or ZDF (*C*) rats were lower for obese compared to lean animals, with statistical significance reaching the pooled samples of ZDF rats, only. On basis of the trends between the calculated means (M) of the individual obese and lean rats, seven out of eight obese Wistar (*A*, green line), five out of seven obese ZF (*B*, blue line) and seven out of eight obese ZDF (*C*, brown line) rats displayed phase shifts and amplitudes, respectively, below the means - 1xSD (M) of their lean counterparts. Conversely, six out of eight lean Wistar (*A*, red line), seven out of eight lean ZF (*B*, pink line) and seven out of eight lean ZDF (*C*, yellow line) rats displayed phase shifts and amplitudes above the means + 1xSD of their obese counterparts.

Comments: Despite the trends between the lean and obese state, only, with regard to the mean phase shift and amplitude, their measurement enabled the differentiation of the majority of individual lean and obese rats irrespective of their genotype. Differentiation between rats of different genotype or body weight required their pairwise comparison using two channels each of the same chip, subsequent regeneration of the chip and its re-use for six cycles *per* animal group (12/6/6 setting).

A closer inspection of the absolute values of both maximal phase shift and minimal amplitude for the individual serum samples within each animal group revealed positive correlations between the degree of the insulin-resistant / diabetic state of the individual rats (as reflected in the fasting plasma insulin levels alone or in combination with the fasting plasma glucose levels) and the decline in phase shift or amplitude. This was true (ranking order according to increasing hyperinsulinemia / hyperglycemia, as indicated (Supplemental Table S2), and decline in phase shift or amplitude) for lean Wistar 6 → 7 → 8 which were distinct from 1, 2, 3, 4 and 5 (S10*A*, see Fig. 5*C, E*), lean ZF 19 → 17 → 21 which were distinct from 18, 22, 23 and 24 (S10*B*, see Fig. 5*E*) and lean ZDF 32 → 34 → 35 which were distinct from 36 to 39 (S10*C*, see Fig. 5*C*) rats as well as for obese Wistar 16 → 12 → 14 which were distinct from 9, 10, 13 and 15 (S10*A*, see Fig. 5*D, F*), obese ZF 30 → 31 → 25 which were distinct from 26 to 29 (S10*B*, see Fig. 5*F, G, H*) and obese ZDF 47 → 46 → 42 which were distinct from 40, 41, and 45 (S10*C*, see Fig. 5*E, G, H*) rats.

Supplemental Figure S11. Effect of GPI-PLD on chip-based sensing of unprocessed serum GPI-AP.

Legend: Serum from lean Wistar rats was incubated (30 min, 30°C) in the absence (C) or presence of the GPI anchor-cleaving GPI-PLD over a wide range of concentrations prior to injection (see Methods). The maximal phase shift (upper panel) and minimal amplitude (lower panel) measured (see Fig. 5) are given as

means ± SD. * $p \leq 0.05$ and # $p \leq 0.01$ between the GPI-PLD and control (incubation with buffer only, C) treatment.

(S11)

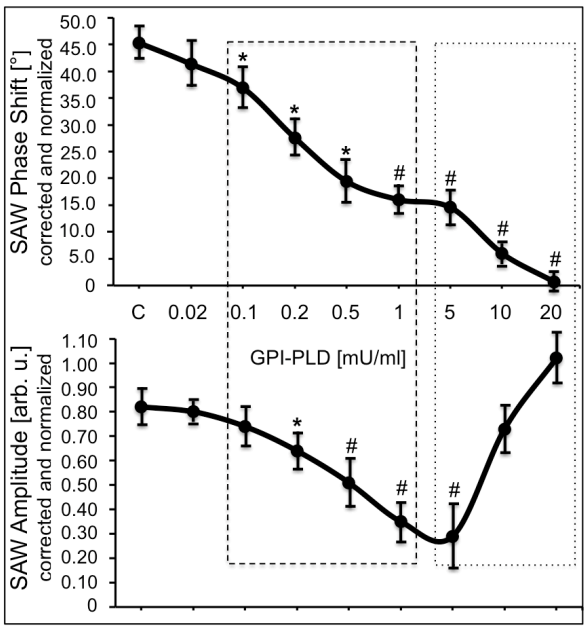

Outcome: At moderate concentrations of GPI-PLD and in consequence upon partial lipolytic removal of the GPI-AP coat, maximal phase shift and minimal amplitude become significantly reduced in concentration-dependent fashion (hatched rectangle) compared to untreated complexes, which can be explained best by decrements in the ratio of GPI-AP protein moieties relative to phospholipids and cholesterol leading to decreased spec. mass or size and elasticity of the unprocessed GPI-AP in complex with lipids. At high GPI-PLD concentrations the total elimination of the GPI-AP from the complexes interferes with their capture and thereby with chip-based sensing as reflected in complete abrogation of complex-induced phase shift and amplitude reduction (punctuated rectangle).

Supplemental Figure S12. Effect of (bio)chemical treatments of unprocessed serum GPI-AP on their differentiation power.

Legend (*A*): Serum samples were incubated with microspheres coupled to α-toxin and BSA as control (filled bars) and then centrifuged (see Methods), or with PI-PLC from *Bacillus cereus* and PC-PLC from *Clostridium perfringens* (known to be ineffective in cleaving GPI anchors) as control (hatched bars) or with 0.05% NP-40 and PBS as control (open bars). The maximal phase shift (upper panel) and minimal amplitude (lower panel) were measured and are given as means of the differences between the paired rat groups from two independent experiments with different chips relative to the corresponding control incubations set at 100%, each.

(S12*A*)

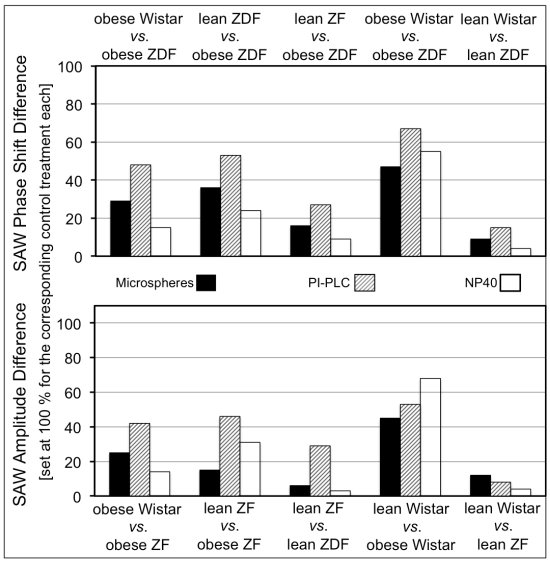

Legend (B): Serum samples were incubated (30 min, 30°C) in the presence of increasing concentrations of the indicated phospholipases (see Methods) or only with the corresponding buffers as control treatments (C). * $p \leq 0.05$ and # $p \leq 0.01$ between phospholipase and (C).

(S12*B*)

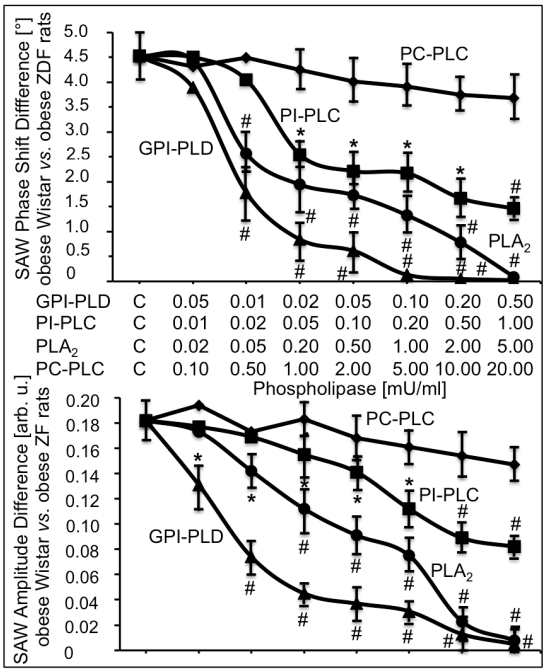

Outcome (*B*): Exposure of the serum samples to PI-PLC from *Bacillus cereus* and GPI-PLD from human serum (at concentrations which do not compromise capture of the unprocessed GPI-AP, see Supplemental Figure S11), both known to cleave the GPI anchor of GPI-AP in the absence and presence of detergent, respectively, and PLA_2 from bee venom, capable of degrading phospholipids within intact membranes, led to concentration-dependent declines of the differences in phase shift (upper panel) and amplitude (lower panel) to up to their complete loss in case of GPI-PLD and PLA_2. In contrast, PC-PLC from *Chlostridium perfringens*,

which does not cleave GPI anchors and presumably has no access to phospholipids in complex with GPI-AP, had no effect at all.

Legend (*C*): Serum samples were subjected to dephosphorylation by hydrogen fluoride (HF), deamination by nitrous acid (NA), proteolysis by proteinase K (PK) and deglycosylation by *N*-glycanase F (Glyc) or α-mannosidase (Man) or to appropriate “mock” treatments (M), which mimick the corresponding treatment conditions without being effective (see Methods), or left untreated as control (C). * $p \leq 0.05$ and $^{\#}$ $p \leq 0.01$ of T *vs*. M.

(S12*C*)

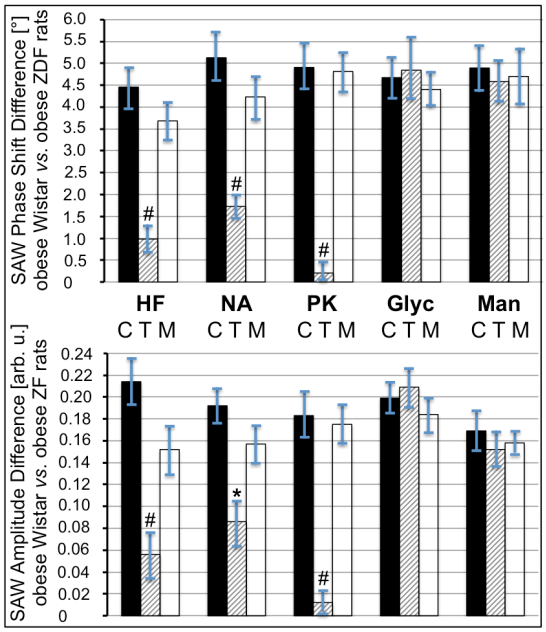

Outcome (*C*): Treatment of the serum samples with hydrogen fluoride and nitrous acid, leading to cleavage of the GPI anchor of GPI-AP at specific sites or with proteinase K for digestion of the protein moiety of GPI-AP provoked significant declines in the phase shift (upper panel) and amplitude (lower panel) differences between obese Wistar and ZDF or ZF rats, respectively, compared to the corresponding "mock" treatment (M). In contrast, incubations with *N*-glycanase F and α-mannosidase, commonly used for trimming of *N*-glycosidic side chains of glycoproteins, were completely ineffective.

Legend (*D*): For pull-down of Gce1 and CD73, serum samples from eight lean Wistar or obese ZDF rats were incubated (30 min, 30°C) in the absence (C) or presence of cAMP or AMP covalently coupled to agarose beads (cAMP, AMP), a combination thereof (cAMP+AMP) or agarose alone (A) and then centrifuged under conditions, which are compatible with maintenance of the complex structure (see Methods). The supernatants were measured (see Figure 5) for maximal phase shift (upper panel) and minimal amplitude (lower panel) and are given as means ± SD. * $p \leq 0.05$ and $^{\#}$ $p \leq 0.01$ between the specific and agarose (A) treatment for a given rat group, § $p \leq 0.05$ between obese ZDF and lean Wistar rats for (C) and (A) treatments, respectively.

(S12*D*)

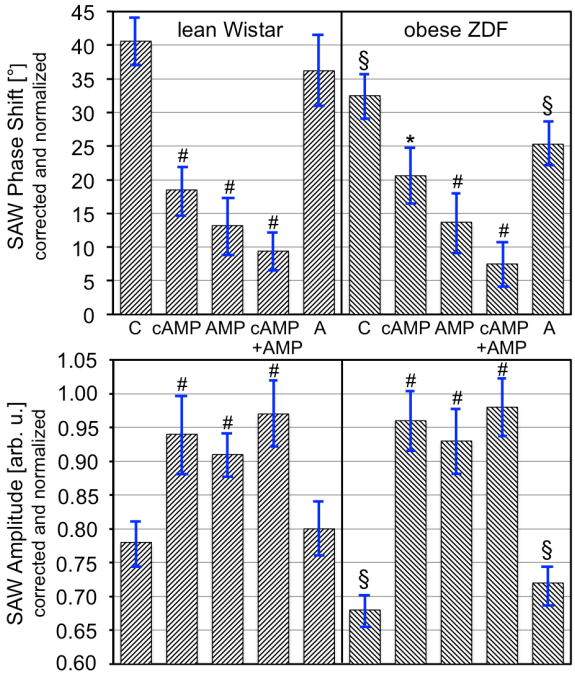

Outcome (*D*): The supernatants from (c)AMP- or cAMP/AMP-agarose-treated sera from both lean Wistar and obese ZDF rats induced significant reductions in phase shift and elevations in amplitude in comparison to supernatants from agarose-treated sera (A) and untreated sera (C) of the corresponding rat group. The minor differences between untreated and agarose-treated sera demonstrated the low unspecific interaction of unprocessed GPI-AP with the agarose beads and thereby argues for the specificity of the depletion procedure for Gce1- and CD73-harboring complexes. The more pronounced but subadditive effect of the combination of cAMP- and AMP-agarose compared to the single treatments hints to the presence of complexes displaying either Gce1 or CD73, as well as those expressing both.

Conclusion (*D*): The GPI-AP Gce1 and CD73 seem to be constituents of serum complexes of high (lean Wistar rats) and low (obese ZDF rats) spec. mass and/or size as well as elasticity, respectively (as reflected in the differences in phase shift and amplitude of C or A between the rat groups).

The concerted function of Gce1 and CD73 in (c)AMP metabolism on the surface of adipocytes leading to degradation of cAMP, which triggers lipolysis, *via* AMP to adenosine, which blocks lipolysis (94-97), may be considered as feed-forward regulation of the insulin-driven incorporation of fatty acids into lipids. In the insulin-resistant hyperinsulinemic state, the diminished release of Gce1 and CD73 into serum complexes (as manifested in their lowered spec. mass, size or/and amount) from the surface of adipocytes would counteract lipolysis through elevated (c)AMP metabolism at the immediate adipose surface area by Gce1 and CD73 retained at the plasma membranes.

The apparent presence of CD73 and Gce1 in serum complexes prompts speculations about the nature of the releasing cells/tissues and about their physiological role in the normal and disease state. The pronounced expression and release of Gce1 and CD73 from primary rat adipocytes in EV in response to metabolic stress (e.g. palmitate, H_2O_2) have previously been demonstrated (4, 18, 19, 46, 98) raising the possibility that adipose tissue operates as source for the released unprocessed GPI-AP. However, an additional and even more critical role of other cells, in particular macrophages, lymphocytes and

reticulocytes, on basis of their relative abundance in blood and proven capability of secreting EV (43, 98, 99) can not be excluded at present.

Legend (*E*): Undiluted serum samples were incubated (30 min, 4°C) in the presence of increasing concentrations of BATC, octylglucoside (OG) and NP-40 as indicated or in the absence of detergent as control (C) and then measured after 10-fold dilution with PBS. To correct for effects of the detergents on the viscosity of the sample fluid, values for PBS containing the same final concentration of detergent were subtracted from the corresponding sample values. * $p \leq 0.05$ and $^{\#}$ $p \leq 0.01$ between detergent and control (C) treatment.

(S12*E*)

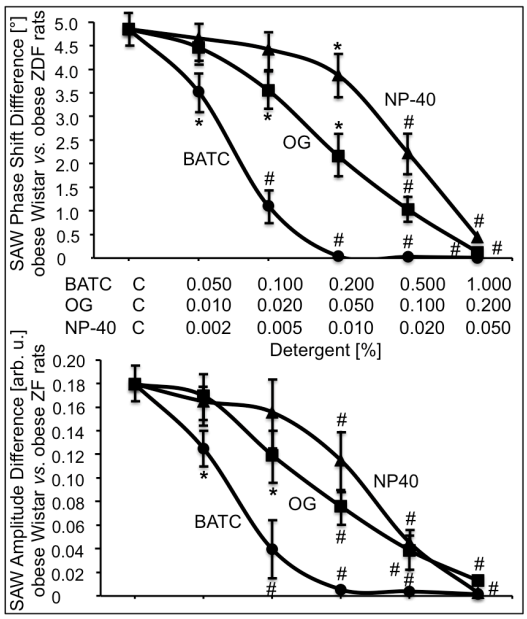

Outcome (*E*): BATC known to induce selective solubilization and enrichment of GPI-AP from plasma membranes (48) as well as OG and NP-40, which efficiently solubilize transmembrane proteins and GPI-AP, caused declines in phase shift and amplitude differences between obese Z(D)F and Wistar rats at concentrations above 0.05, 0.02 and 0.01%, respectively.

Conclusions: The biochemical treatment of the serum samples by (i) lipolytic or chemical (hydrogen fluoride dephosphorylation, nitrous acid deamination) cleavage of the GPI anchor (Supplemental Figures 11, 12*A*-*C*), (ii) adsorption to microspheres coupled to α-toxin or (c)AMP for depletion of complexes equipped with GPI-AP or (c)AMP-binding proteins, such as the GPI-AP, CD73 and Gce1, respectively (Supplemental Figure 12A, D), and (iii) various detergents (Supplemental Figure 12*A, E*) or cholesterol-extracting agents (Supplemental Table S5) for release of lipidic constituents revealed that serum complexes which are constituted by GPI-AP, among them CD73 and Gce1, phospholipids and cholesterol, are responsible for the differentiation of rats according to the genotype and metabolic state using chip-based sensing.

Supplemental Figure S13. Determination of thresholds for the differentiation of serum complexes from rats of different metabolic state.

Rationale: The data presented so far raise the question about the nature of the appropriate "control", i.e. whether samples from T2D patients have to be compared with those from "healthy" probands of matched genotype or metabolic state (body weight, plasma insulin) or, alternatively, with pooled serum samples from randomly collected subjects. Furthermore, for clinical throughput analysis, the pairwise comparative measurements would be time-consuming and expensive.

Legends (*A, B*): The maximal phase shift (*A*) and minimal amplitude (*B*) were measured for the pooled serum samples from eight lean and obese Wistar, ZF or ZDF rats (see Fig. 5*A*). Importantly, prior to measurement, the sera were subjected to 12 vibration cycles (hatched bars) or left untreated (filled bars). For calculation of the effects specifically provoked by (vibration-sensitive) complexes, the corrected and normalized phase shift of the vortexed sample was subtracted from that of the untreated sample (*A*, open bars) and, correspondingly, the difference between the corrected and normalized amplitude of the vortexed sample and that of the untreated sample was subtracted from the starting amplitude which was set at 1.0 (*B*, open bars). Phase shift and amplitude are given as means ± SD from four to six independent experiments with the untreated and vortexed samples, each, using four channels each, which were re-used six times for successive analysis of samples from obese ZDF, obese ZF, obese Wistar, lean ZDF, lean ZF and lean Wistar (in that order) with the same channel. Arrows indicate the decline of the phase shift and amplitude exerted by vibration-sensitive complexes (open bars) from lean Wistar to up to obese ZDF rats. * $p \leq 0.01$ and $^{\#}$ $p \leq 0.05$ for vibration-sensitive complexes (open bars) *vs*. serum of rats of either identical genotype or similar body weight.

(S13*A*) **(S13*B*)**

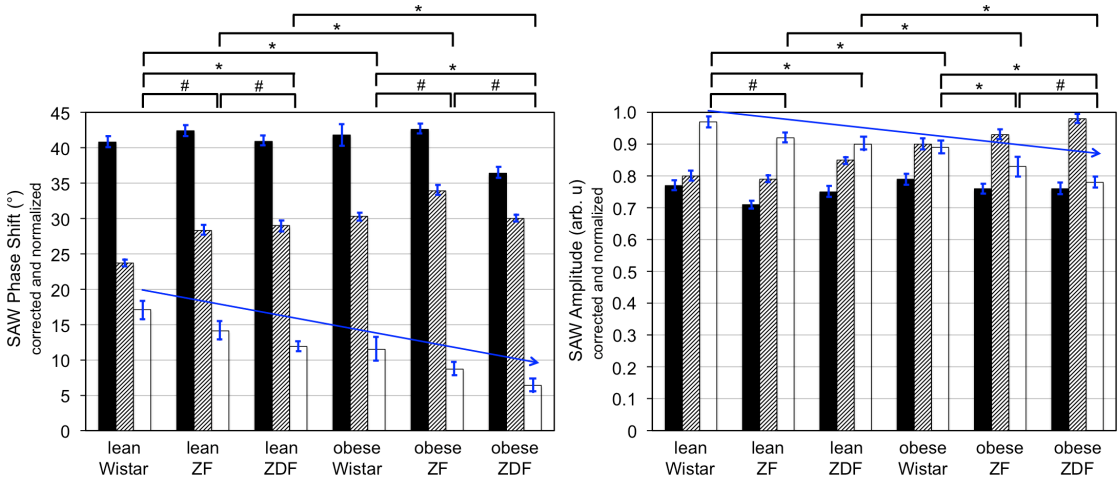

Outcome (*A, B*): Determination of neither the total (i.e. complex- *plus* non-complex-induced)(filled bars) nor the non-complex-induced (hatched bars) phase shift and amplitude supported differentiation of the rat sera according to genotype or body weight. However, the complex-induced (open bars) phase shift (*A*) as well as amplitude (*B*) significantly declined from lean Wistar, ZF and ZDF to obese Wistar, ZF and ZDF rats (in that ranking order). Thus, stable complexes, which are present in rat serum and resist mechanical forces and may be identical with, but not restricted to EV, apparently are not correlated to genotype and body weight. Their effect on phase shift and amplitude have to be eliminated to unmask the labile complexes for

differentiation between distinct genotypes and body weights. In conclusion, calculation of the complex-mediated effects as the difference (open bars) between the total (filled bars) and the non-complex-mediated alterations (since unaffected by vibration, hatched bars) in phase shift (*A*) and amplitude (*B*) enables the consistent differentiation of the sera according to genotype and body weight. Future cross-sectional and longitudinal studies using randomly collected rat cohorts and relying on the presented experimental protocol and threshold values for phase shift and amplitude have to demonstrate whether chip-based sensing of serum complexes enables the differentiation of metabolic states for monitoring of pre-diabetic states.

Supplemental Figure S14. Impact of genotype, metabolic state and age of rats on the differentiation potential of unprocessed GPI-AP derived from plasma membranes.

Legend: The experiment was performed (see Fig. 3) with plasma membranes prepared from total adipocytes of lean (open bars) and obese (hatched bars) Wistar, ZF and ZDF rats as well as of young (filled bars) and old (squared bars) Wistar rats or from small adipocytes of young rats (filled bars) and large adipocytes of old Wistar rats (squared bars) and using 200 µl/min flow rate during Step B (3000-6600 sec). Specific GPI-AP-induced phase shift (*A*) and amplitude reduction (*B*) derived from three independent experiments with measurements in duplicate are given as means ± SD with significant differences indicated (* $p \leq 0.05$, # $p \leq 0.01$).

(S14*A*) **(S14*B*)**

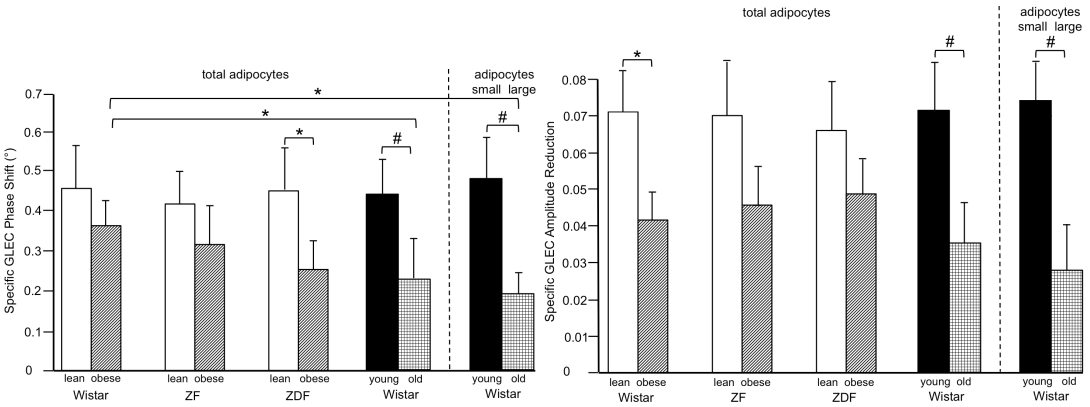

Outcome: On basis of the (significantly) lower phase shifts (*A*) and amplitude reductions (*B*), specifically induced by obese *vs*. lean Wistar, ZF and ZDF rats, plasma membranes from obese rats apparently release complexes of diminished spec. mass, size or amount and viscosity, respectively, compared to those from their lean counterparts. More pronounced differences were observed for old *vs*. young Wistar rats, irrespective of whether the plasma membranes had been prepared from total adipocytes or from large and small adipocytes of old and young rats, respectively. Strikingly, on basis of phase shift measurement, it was possible to differentiate between old (42 weeks, 453-491 g) and obese (9 weeks, 478-545 g) Wistar rats using the corresponding plasma membranes from the total adipocytes (i.e. without size separation).

Conclusion: Plasma membranes from adipocytes of lean *vs*. obese and young *vs*. old rats differ in the potential to release complexes of unprocessed GPI-AP and lipids in the "lab-on-the-chip" configuration with regard to their amount and/or structure.

Supplemental Figure S15. Impact of albumin on the differentiation potential of unprocessed GPI-AP derived from plasma membranes *in vitro*.

Rationale: The findings that exposure of the immobilized plasma membranes towards BSA fosters the release of unprocessed GPI-AP (see Supplemental Figure S6) prompted to study whether this differentiation becomes more pronounced in the presence of BSA in the running buffer during Step B.

Legend: The experiment was performed in the absence (open bars) or presence of 0.2% BSA (filled bars). The differences (means ± SD with * $p \leq 0.05$, # $p \leq 0.01$) in specific GPI-AP-induced phase shift (*A*) and amplitude reduction (*B*) between lean and obese (on the basis of total adipocytes) as well as young and old rats (on the basis of total adipocytes or small/large adipocytes from young/old rats) were calculated for the generation of the plasma membrane-derived unprocessed GPI-AP in the absence or presence of BSA, each.

(S15*A*) **(S15*B*)**

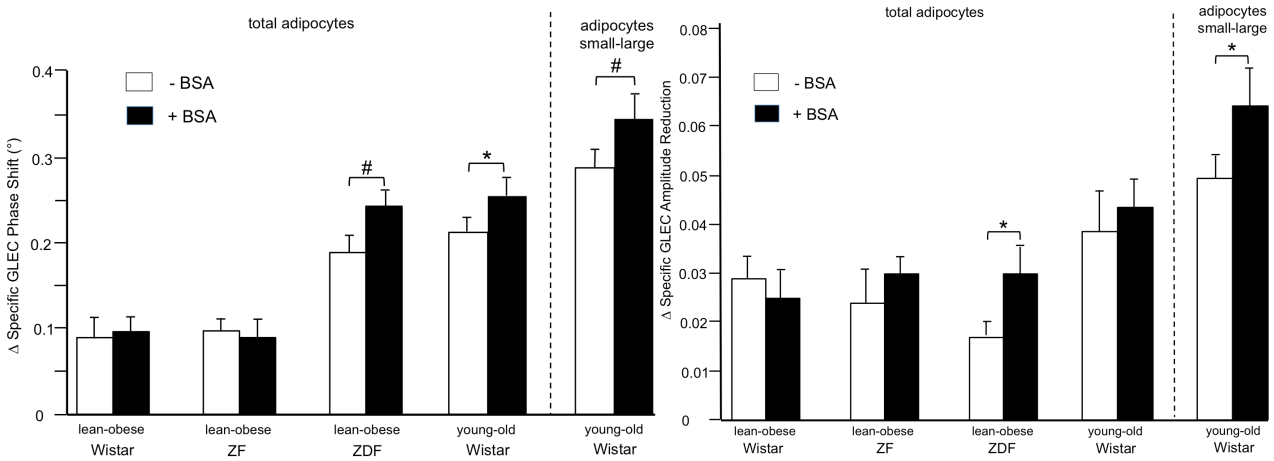

Outcome: Both specific phase shift (*A*) and amplitude reduction (*B*) were significantly reduced for total adipocytes from obese *vs*. lean ZDF rat and old *vs*. young Wistar rats as well as for small adipocytes from young *vs*. large adipocytes from old Wistar rats. Remarkably, isolated adipocyte plasma membranes of obese and old Wistar rats were differentiated from one another on basis of the specific phase shift induced by the unprocessed GPI-AP upon release from them (*A*).

Conclusion: The (significantly) more pronounced differences in phase shift and amplitude reduction between lean and obese ZDF as well as young and old Wistar rats in the presence of BSA may be explained by facilitation of the generation of unprocessed GPI-AP from immobilized rat adipocyte plasma membranes, which is predominantly driven by the microfluidic buffer stream passing the chip channels, through "extraction" by BSA. The finding suggests that the use of BSA during “lab-on-the-chip” analysis of plasma membrane-derived complexes of unprocessed GPI-AP and lipids improves the differentiation between donor rats with different genotype and body weight. Thus both adipocyte plasma membrane-derived and serum complexes, as monitored by chip-based sensing, are affected by the metabolic state of the corresponding donor rats in similar fashion.

Supplemental Figure S16. PIG37-dependent sensing of unprocessed GPI-AP in serum of control subjects and diabetic patients.

Legend: 40 µl of pooled serum sample diluted five-fold with PBS were injected into α-toxin-coated or "blank" channels at a flow rate of 80 µl/min and at 20°C using running buffer (period A0). Following washing by

injection of 170 µl of running buffer at a flow rate of 200 µl/min and 37°C, 280 µl of 400 nM annexin-V containing 40 µM Ca^{2+} were injected at a flow rate of 120 µl/min (period A1). Subsequently, the channels were rinsed with 230 µl of running buffer at a flow rate of 200 µl/min and 37°C, followed by injection of 130 µl of 30 µM PIG37 at a flow rate of 30 µl/min (period B) and then of 230 µl of running buffer at a flow rate of 200 µl/min. Regeneration of the chips was accomplished by sequential injection of 180 µl of 200 µM PIG41 at a flow rate of 60 µl/min and 37°C (period C), then of 200 µl of running buffer at a flow rate of 200 µl/min and finally of 900 µl of running buffer containing 0.2 mM EGTA and 0.05% NP-40 at a flow rate of 200 µl/min (period D). Phase shift (as °) and amplitude (as arb. u.) are given upon correction for the "blank" and "albumin" channels and normalization (set at 0° and 1 arb. unit, respectively, for start of the injection at 0 sec) as original data. Representative overlay diagrams from three independent measurements (as indicated by distinct colors) using distinct channels of the same chip are shown. The maximal phase shifts and minimal amplitudes, respectively, measured at the end of the consecutive injection of annexin-V + Ca^{2+} (period A1) and PIG37 (period B) are indicated as hatched lines. These PIG37-dependent changes in phase shift and amplitude are marked by triangles for each serum sample. Δ / - Δ indicates increase / decrease of phase shift or amplitude in comparison to the absence of PIG37 (i.e. difference between end of period B and A1). A, G, B, H, E: Control persons; D, I, F, C, K: Diabetic patients.

(S16)

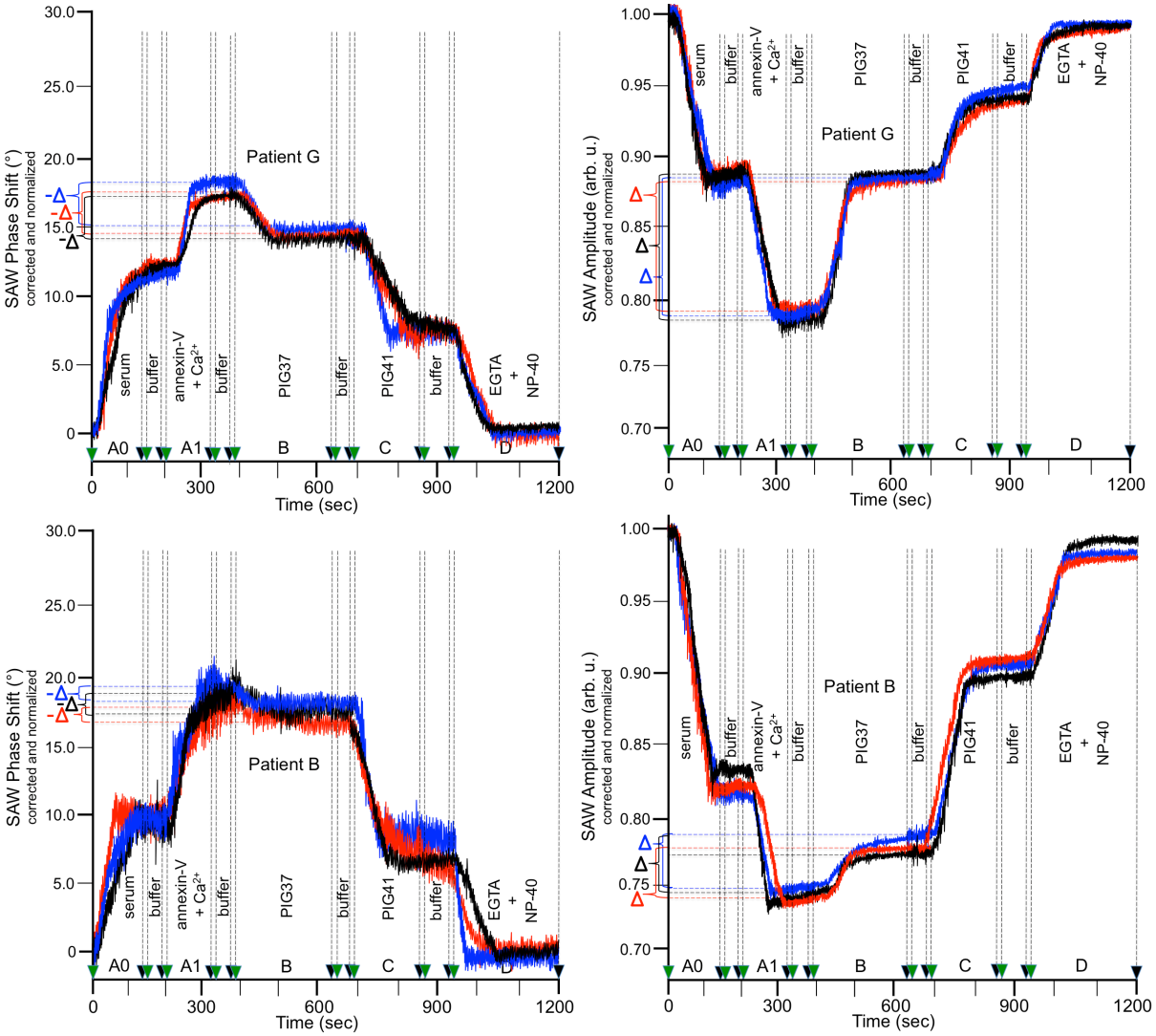

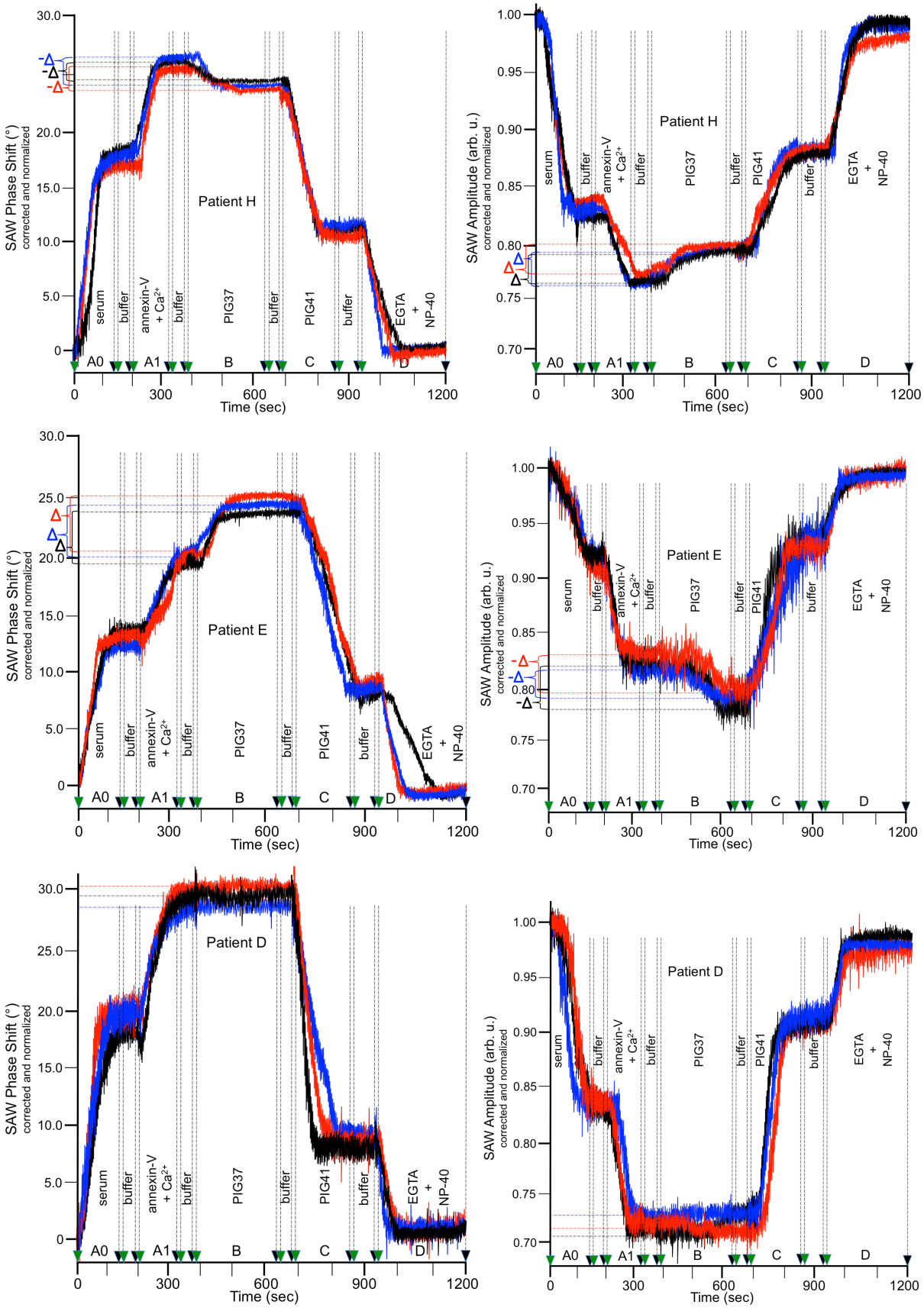
Patient H
Patient E
Patient D
SAW Phase Shift (°)
corrected and normalized
SAW Amplitude (arb. u.)
corrected and normalized
Time (sec)
serum
buffer
annexin-V
+ Ca2+
PIG37
PIG41
EGTA
+
NP-40
A0
A1
B
C
D

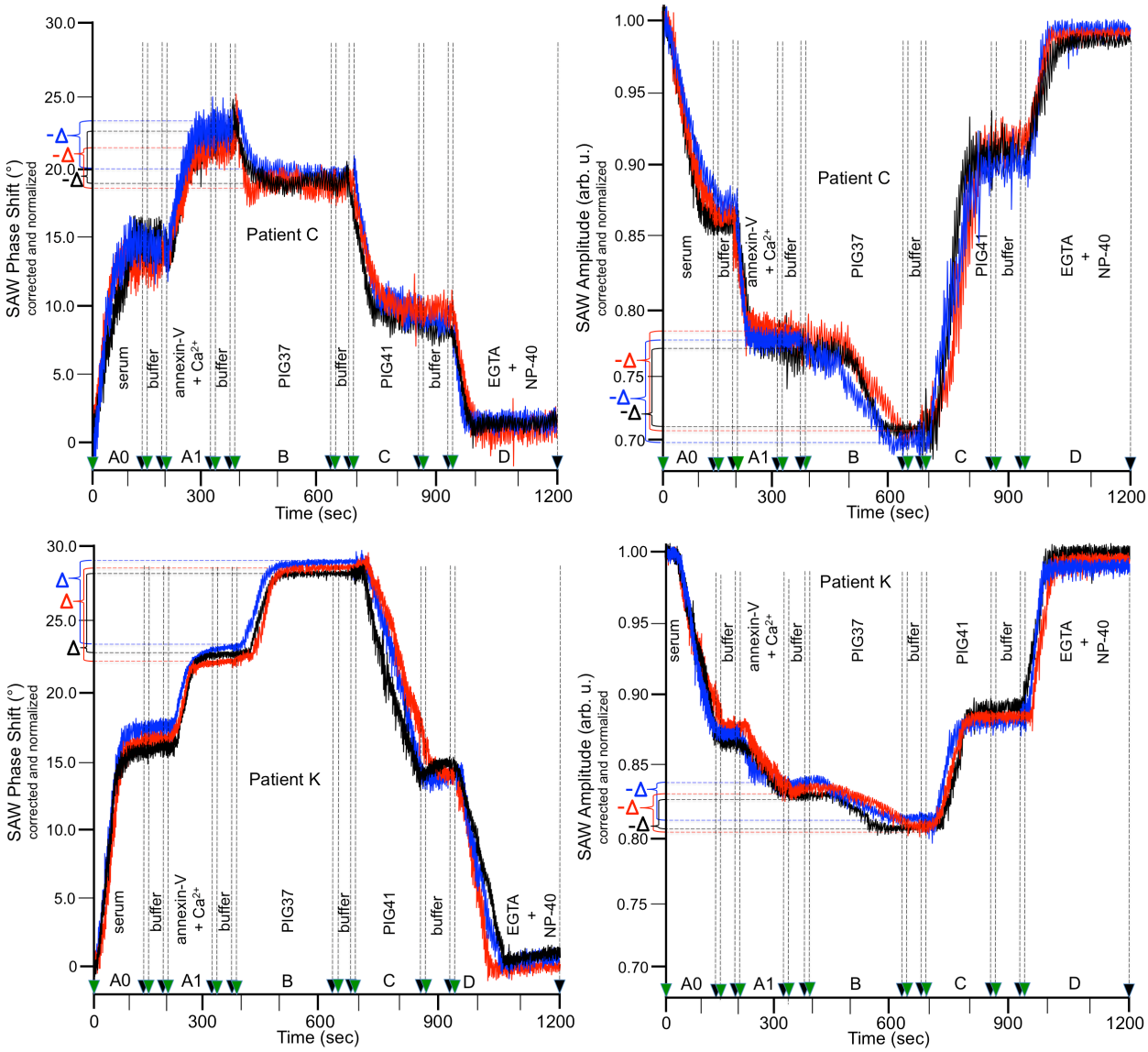

Outcome: Chip-based sensing confirmed the presence of unprocessed GPI-AP in each individual serum sample based on the considerable phase shift increases and amplitude reductions upon injection of serum (capture of the GPI-AP) and annexin-V/Ca^{2+} (detection of the complexes of GPI-AP and lipids) as well as the abrogation of these changes upon injection of PIG41 (competitive displacement of the GPI-AP/complexes) and EGTA+NP-40 (regeneration of the chip). Moreover, measurement of each sample in triplicate revealed the high reproducibility of the measurement. Interestingly, the extent of the phase shift increases and amplitude reductions induced by identical serum volumes differed between the individuals to a varying degree. However, no correlation was found between the extent of the phase shift increases or amplitude reductions and the metabolic (T2D, T1D, normal) state of the probands as manifested in the HbA1c level and body weight (Supplemental Table S7). Most importantly, the same was true for the PIG37-dependent changes in phase shift and amplitude (see also Fig. 9*C*), which are critical for the differentiation of the unprocessed GPI-AP in serum of rats of different genotype and similar body weight and *vice versa* of identical genotype and differing body weight (see Fig. 5). In particular, PIG37-dependent phase shift decrease was very pronounced with sample A (control subject) and sample C (T1D patient), very low and even absent with sample B (control subject) and sample D (T1D patient), respectively. Conversely, both sample E (control subject), sample F (T2D patient) and sample K (T1D patient) displayed pronounced

PIG37-dependent upregulation of phase shift. (Marked) PIG37-dependent increase in amplitude was measured with control subjects (samples A, G, B, H), only, whereas decrease or no effect in response to PIG37 became evident for control subjects (sample E) and T1D (samples D, C, K) and T2D (sample I, F) patients. In apparent contrast to these results of the PIG37-dependent sensing of unprocessed GPI-AP in serum of humans, the comparative analysis of between rats of identical genotype and different body weight as well as different genotype and similar body weight (Fig. 5C-H, Supplemental Figures S9, S10*A*-*C*) unravelled decreases in PIG37-dependent phase shift as well as amplitude, exclusively, for the hyperinsulinemic (normo- or hyperglycemic) *vs*. the normoinsulinemic or mildly hyperinsulinemic (normoglycemic) state.

Supplemental Figure S17. Effect of mechanical treatment of human serum complexes on PIG37-dependent phase shift and amplitude changes.

Legend: The PIG37-dependent phase shift and amplitude changes were determined as described above (Supplemental Figure S16) for three individual human serum samples (crossings, proband A; triangles, proband B; squares, proband C). Effect of (*A*) sample processing and storage; (*B*) temperature; (*C*) centrifugation; (*D*) ultrasonic waves; (*E*) vibration.

(S17*A*) **(S17*B*)**

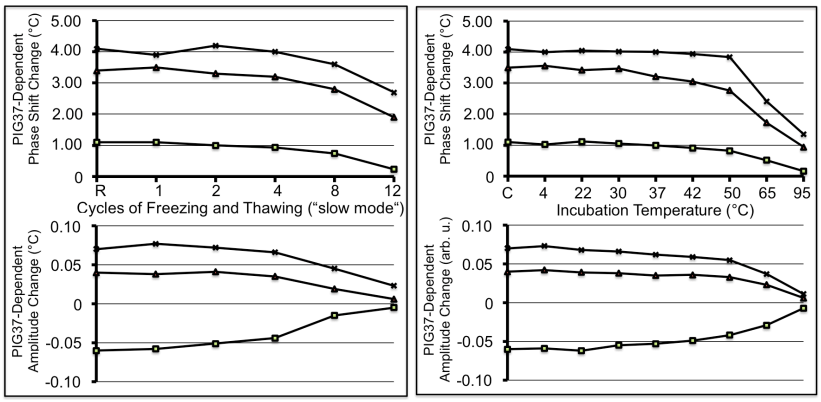

(S17*C*) **(S17*D*)** **(S17*E*)**

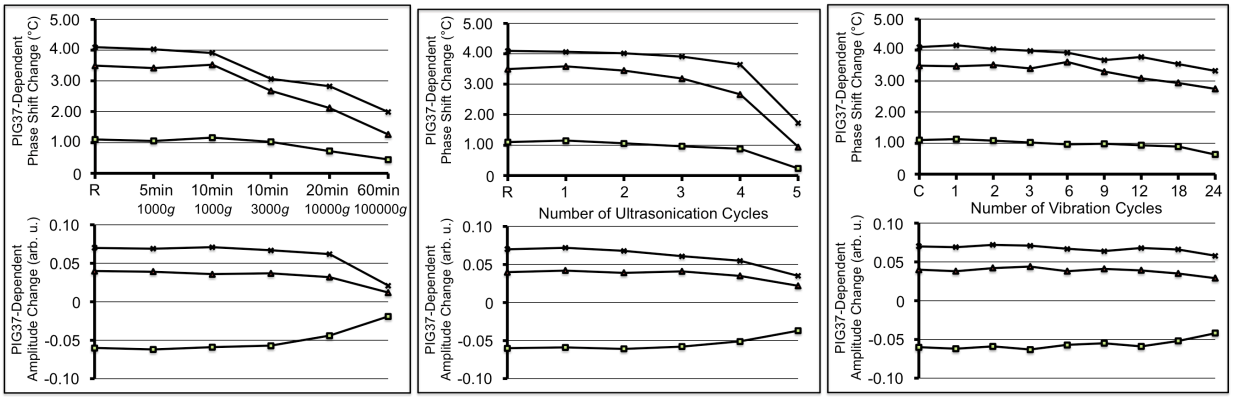

Outcome: Information about the physical stability of the complexes of GPI-AP and lipids in human serum *per se* and differences herein between humans and rats was obtained by exposure of human serum to mechanical treatments prior to measurement as described for rat serum samples (see Fig. 7). For each treatment, marked declines to up to complete abrogation of the PIG37-dependent changes in phase shift as

well as amplitude for each individual sample were observed only under the most extreme conditions. This is in contrast to the exquisite lability of the rat complexes upon exposure to the same treatments.

Supplemental Figure S18. Hypothetical model for the release and degradation of unprocessed GPI-AP in serum of normal and insulin-resistant/diabetic rats and their analysis by chip-based sensing. (*A*) In the normoinsulinemic normoglycemic state of (wildtype) rats, the expression of high cholesterol lipid rafts favors the release of unprocessed GPI-AP (thick arrow). Several configurations of the constituents within the complexes of GPI-AP and lipids are conceivable: Fragments from the extracellular plasma membrane leaflet encompassing a single or a few lipid raft(s) may form "open phospholipid monolayer sheets" initially. In course of release or shortly thereafter they may acquire a "closed" micelle-like structure spontaneously or upon incorporation of additional constituents or in course of fusion with other "sheets" in the blood. Alternatively, sequential bulbing, incision and fusion of the extracellular leaflet of plasma membranes at high cholesterol lipid rafts may result in the separation from the donor cell of "closed" micelle-like structures harboring the unprocessed GPI-AP and lipids. Importantly, for each of these mechanisms the membrane rigidity at high cholesterol lipid rafts may control the rate of the spontaneous as well as controlled release of the unprocessed GPI-AP in positive fashion, either through stabilization and extrusion of "open sheets" or through facilitation of the shaping of "closed" micelles. The impact of the plasma membrane cholesterol content and thereby rigidity *vs*. fluidity of lipid rafts on their functionality has previously been underscored by the demonstration of a correlation between cholesterol deprivation from lipid rafts and impairment of insulin signal transduction *via* the lipid raft-associated insulin receptor in rat adipocytes (99-101). **Inset** Detection of unprocessed GPI-AP in serum from normal rats (green curve) by chip-based sensing in comparison to buffer alone (grey curve) reveals (i) a pronounced SAW phase shift (red righwarded arrow) due to capture of complexes of GPI-AP and lipids of certain spec. mass / size and/or at a certain number and (ii) a small reduction in the SAW amplitude (blue downwarded arrow), only, due to capture of complexes of high elasticity and low viscosity (for symbols see *B*).

(S18A)

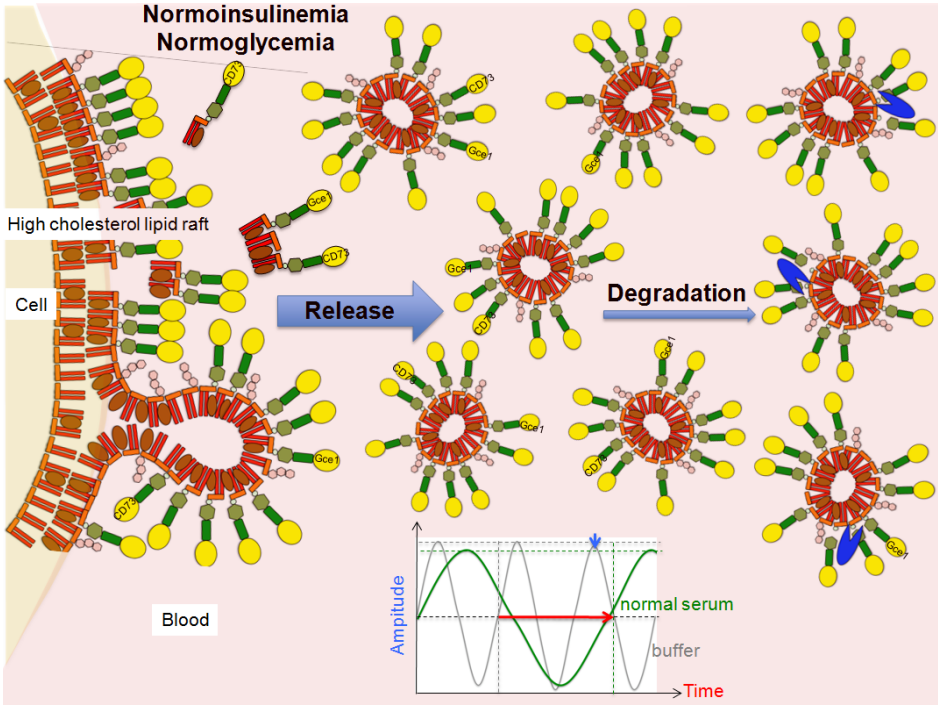

(*B*) In the hyperinsulinemic (hyperglycemic) state of obese Wistar and ZF (ZDF) rats, low cholesterol lipid rafts, formed from the high cholesterol lipid rafts, release of complexes of GPI-AP and lipids of reduced spec. mass / size and/or at reduced number (thin arrow). It has been proposed that during intensive synthesis of triglycerides and accompanying biogenesis of lipid droplets in enlarging adipocytes, cholesterol is translocated from plasma membrane lipid rafts as its major storage site in small adipocytes to the emerging lipid droplets for insertion into their outer phospholipid monolayer (99-101). This inevitably leads to transient depletion of cholesterol from lipid rafts. With regard to adipocytes, at least, this molecular mechanism driven by insulin stimulation of lipid synthesis could induce the transformation of high cholesterol lipid rafts in the plasma membranes of normoinsulinemic normoglycemic rats into low cholesterol lipid rafts of hyperinsulinemic (hyperglycemic) rats. Thereby, the release of complexes into blood would be coupled to the metabolic state *via* the cholesterol content of the plasma membrane lipid rafts of the releasing cell with the higher the insulin plasma level, the lower/higher the amount of high/low cholesterol lipid rafts and the lower the efficacy of release of the complexes. It remains to be clarified whether a similar mechanism could explain the apparent transfer of GPI-AP between cells *in vivo* which has been implicated a physiological role in intercellular communication (102-108). **Upper inset** Detection of unprocessed GPI-AP in serum of hyperinsulinemic rats (green curve) by chip-based sensing in comparison with buffer alone reveals (grey curve) (i) a small SAW phase shift only (red righwarded arrow) due to capture of complexes of GPI-AP and lipids of reduced spec. mass / size and/or at diminished number and (ii) a pronounced reduction in the SAW amplitude (blue downwarded arrow) due to capture of complexes of low elasticity and high viscosity. **Lower inset** The direct comparison of serum between hyperinsulinemic and normoinsulinemic (normal) rats demonstrates for the former the considerably reduced phase shift (red leftwarded arrow) due to downregulated spec. mass / size and/or number in parallel to the diminished amplitude (downwarded blue arrow) due to elevated viscosity of the complexes with incomplete GPI-AP coat compared to the many large complexes with complete GPI-AP coat in normoinsulinemic rats.

(S18B)

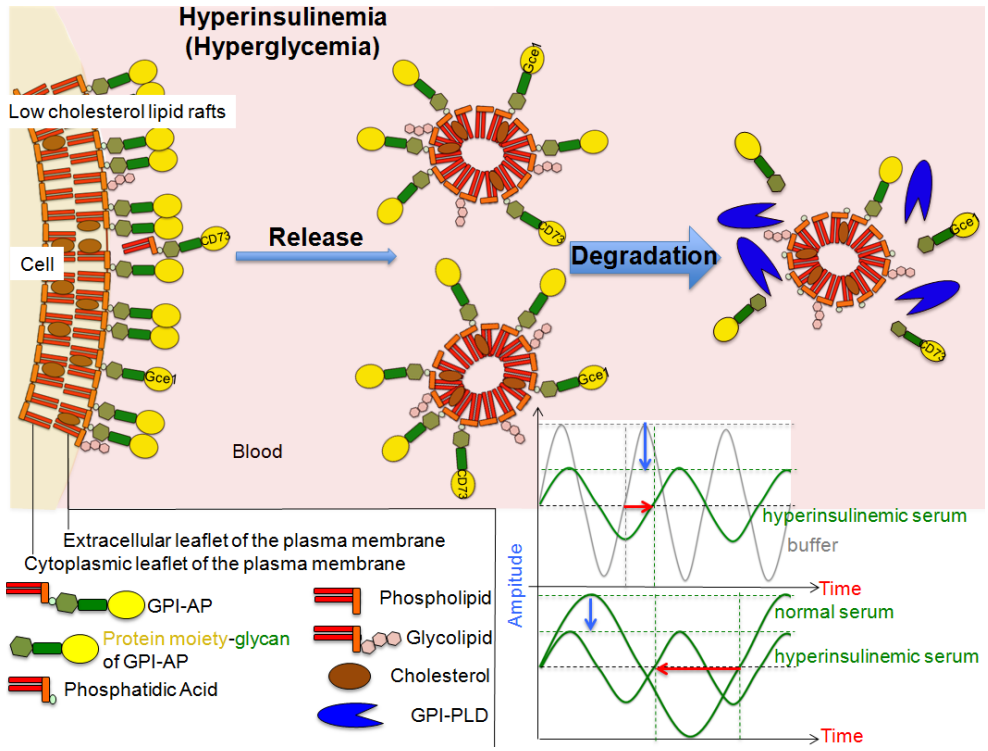

Final Conclusion

The findings represent an example for the fruitfulness of the "correlation-is-enough" or "end-of-theory" hypothesis (109). The use of a minimal bias, i.e. unprocessed GPI-AP are susceptible to membrane release on basis of their amphiphilicity, in combination with an appropriate state-of-the-art detection method, i.e. chip-based sensing relying on surface acoustic waves, may lead to the elucidation of a phenomenon of apparent (patho)physiologial relevance and putative medical application (prediction and stratification of metabolic diseases) without the need for any additional preformed opinions or for (exact) knowledge of the underlying structures (of the GPI-AP in complex with lipids) and molecular mechanisms (mediating their release and linkage to [patho]physiological correlates or endpoints). The approach just relies on the production of (complex) signals (signatures) by an instrument and their correlation to phenotypic states. Thus the present study demonstrates that the chip-based sensing technology enables *per se* the measurement of the apparent instability of certain plasma membrane components in response to intrinsic and extrinsic stimuli, which encompass, but may not be restricted to, the genotype and metabolic state of the donor organism. It is this combination of a novel technique (surface acoustic waves) and a minimal bias (biophysical characteristics of GPI-AP) enabling the measurement of a cell biological phenomenon of potential broad interest (instability of plasma membrane components).

SUPPLEMENTAL TABLES S1-7

Supplemental Table S1. *Characterization of the rat adipocytes used for preparation of the medium samples.*

Legend: Isolated rat adipocytes of small, medium and large size were prepared and assayed at identical lipocrit for insulin-stimulated lipogenesis as the incorporation of fluorescently labeled NBD-FA into total neutral lipids in the absence or presence of increasing concentrations of human insulin using TLC and fluorescence scanning (see Methods). Four to six distinct adipocyte preparations and size separations from male rats with incubations in the presence of NBD-FA at each insulin concentration in quadruplicate and TLC analyses in triplicate, each, were performed. The amount of total fluorescent neutral lipids measured is given as means ± SD upon normalization for small adipocytes in the absence of insulin (basal lipogenesis set at 1 arb. unit). Fold-stimulation was calculated as ratio between maximal (presence of 5 nM insulin) and basal lipogenesis (absence of insulin). The EC_{50} values were derived from the corresponding insulin concentration-response curves. $p \leq 0.05$ for $^{\#}$ medium *vs*. small, * large *vs*. medium, § large *vs*. small.

Adipocyte size	**small**	**medium**	**large**
Diameter [µm]	< 75	75 - 150	> 400
Basal lipogenesis	1.00 ± 0.13	2.41 ± 0.32$^{\#}$	5.42 ± 1.83§
Max. lipogenesis	19.63 ± 2.39	29.04 ± 2.97$^{\#}$	12.31 ± 2.55*§
Fold stimulation	19.63 ± 1.77	12.05 ± 2.52$^{\#}$	2.29 ± 0.48*§
EC_{50} [nM]	0.083 ± 0.021	0.286 ± 0.081$^{\#}$	0.594 ± 0.10*§

Supplemental Table S2. *Characteristics of the lean and obese Wistar and Z(D)F rats.*

Genotype	Feeding	No.	Weight [g]	Age [weeks]	Fasting plasma glucose [mM]	Fasting plasma insulin [µg/l]	Metabolic State
Wistar	lean	1	314.9	9	5.56	0.50	normo-
		2	344.9	9	6.16	0.63	insulinemic
		3	324.4	9	6.16	0.50	normo-
		4	334.7	9	6.05	0.50	glycemic
		5	340.1	9	6.77	0.57	
		6	348.6	9	6.60	0.91	
		7	340.2	9	7.92	1.32	
		8	346.2	9	7.15	1.57	
		Mean	**336.8**		**6.55**	**0.74**	
	obese	9	497.5	9	5.96	1.34	mildly
		10	507.9	9	6.73	0.98	hyper-
		11	471.3	9	6.46	1.82	insulinemic
		12	552.5	9	7.05	2.37	normo-
		13	503.2	9	6.87	1.10	glycemic
		14	456.0	9	7.61	2.55	
		15	535.9	9	6.80	0.95	
		16	562.1	9	6.53	1.94	
		Mean	**510.8**		**6.75**	**1.63**	
ZF	lean	17	455.0	42	5.67	0.94	normo-
		18	470.0	42	5.61	0.69	insulinemic
		19	455.0	42	5.94	0.94	normo-
		20	455.0	42	5.56	<0.5	glycemic
		21	494.0	42	5.72	1.21	
		22	434.0	42	5.67	0.58	
		23	475.0	42	5.34	0.65	
		24	430.0	42	6.16	XXX	
		Mean	**458.5**		**5.71**	**0.84**	
	obese	25	566.0	42	5.45	3.79	hyper-
		26	631.0	42	5.56	2.74	insulinemic
		27	644.0	42	5.50	3.22	normo-
		28	653.0	42	5.83	2.86	glycemic
		29	660.0	42	6.05	2.16	
		30	700.0	42	5.72	3.28	
		31	668.0	42	5.83	3.28	
		Mean	**646.0**		**5.71**	**3.05**	
ZDF	lean	32	356.8	14	5.82	0.83	mildly
		33	349.9	14	5.43	0.93	hyper-
		34	355.4	14	5.49	1.56	insulinemic
		35	359.9	14	5.36	1.04	normo-
		36	361.4	14	5.78	0.94	glcemic
		37	379.0	14	5.77	1.52	
		38	383.0	14	5.93	0.85	
		39	360.8	14	5.71	0.50	
		Mean	**363.3**		**5.66**	**1.02**	
	obese	40	376.6	14	22.91	1.89	hyper-
		41	404.9	14	22.56	1.44	insulinemic
		42	437.7	14	21.09	2.85	hyper-
		43	404.4	14	23.06	2.12	glycemic
		44	446.7	14	19.46	1.97	
		45	398.3	14	22.80	1.46	
		46	408.2	14	25.39	1.88	
		47	449.4	14	18.23	2.47	
		Mean	**415.8**		**21.94**	**2.01**	

Comments: Obese ZF rats exhibit about two-fold elevated fasting plasma insulin levels compared to obese Wistar rats and normal fasting plasma glucose levels indicative for their hyperinsulinemic insulin-resistant, but normoglycemic non-diabetic state. At variance, obese ZDF rats are characterized by moderately increased and even lower fasting plasma insulin levels compared to obese Wistar rats and obese ZF rats, respectively, but suffer from fasting plasma glucose levels exceeding those of obese Wistar rats and obese ZF rats by about three-fold and four-fold, respectively. Thus, obese ZDF rats can be regarded as a model for pronounced hyperglycemia and mild hyperinsulinemia with relative insulin deficiency, which is typical for the metabolic stage prior to further impairment and finally complete loss of ß-cell function and development of frank T2D.

Supplemental Table S3. *Comparative measurement of the same serum samples using two different sensing instruments of the same type.*

Legend: Serum from rats of similar body weight and different genotype as well as of identical genotype and different body weight were measured with sensing instruments A and B in pairwise combinations. Maximal phase shift and minimal amplitude were measured (see Fig. 5) and are given for the comparison between individual sera from eight rats as means (M) thereof or for the pooled samples (P)(bold digits) ± SD (thin digits) using one chip for each rat group (12/4 setting) and four to six re-uses. * $p < 0.05$ for lean ZF/ZDF *vs*. lean Wistar, obese ZDF *vs*. obese ZF/Wistar, obese ZF *vs*. obese Wistar, obese ZDF *vs*. lean ZDF).

			Lean						**Obese**					
			Wistar		**ZF**		**ZDF**		**Wistar**		**ZF**		**ZDF**	
			A	B	A	B	A	B	A	B	A	B	A	B
Lean	**Wistar**	M			**0.69*** 0.069	**0.74*** 0.096	**35.1*** 1.14	**31.8*** 1.32	**0.752** 0.095	**0.813** 0.104				
		P			**0.71*** 0.093	**0.79*** 0.119	**36.4*** 0.36	**33.8*** 0.49	**0.703** 0.058	**0.792** 0.087				
	ZF	M	**0.784** 0.065	**0.869** 0.091			**40.50** 4.41	**37.72** 5.04			**0.697** 0.079	**0.748** 0.095		
		P	**0.799** 0.013	**0.893** 0.036			**40.98** 1.82	**39.03** 2.44			**0.725** 0.029	**0.806** 0.037		
	ZDF	M	**39.96** 2.24	**35.72** 2.01	**41.62** 3.76	**38.55** 3.39							**35.77** 2.22	**33.07** 3.11
		P	**40.98** 0.57	**35.04** 0.46	**41.83** 1.68	**37.30** 1.80							**36.8*** 1.53	**34.7*** 2.06
Obese	**Wistar**	M	**0.850** 0.048	**0.931** 0.089							**0.67*** 0.023	**0.76*** 0.040	**33.6*** 1.65	**30.7*** 1.98
		P	**0.819** 0.017	**0.902** 0.054							**0.70#** 0.014	**0.81#** 0.030	**34.7*** 0.57	**32.1*** 0.92
	ZF	M			**0.797** 0.048	**0.832** 0.076			**0.776** 0.054	**0.812** 0.073			**37.48** 2.99	**34.98** 2.40
		P			**0.819** 0.030	**0.889** 0.063			**0.807** 0.011	**0.859** 0.020			**38.4*** 0.87	**36.1*** 0.73
		M											**0.723** 0.081	**0.802** 0.088
		P											**0.76*** 0.031	**0.831** 0.053
	ZDF	M					**40.45** 2.47	**38.78** 3.19	**40.17** 2.24	**37.83** 1.91	**42.09** 1.36	**39.83** 1.81		
		P					**40.13** 0.59	**37.95** 1.06	**41.54** 0.77	**39.50** 1.07	**41.99** 0.54	**40.47** 1.03		
		M									**0.800** 0.057	**0.895** 0.079		
		P									**0.856** 0.013	**0.940** 0.025		

Supplemental Table S4. *Characteristics of the lean, obese, vitamin-supplemented, HFD, YGB and VSG rats and the amplitudes measured.*

Legend: Animal housing and feeding, dietary regimen, surgical procedures, post-operative care and handling and storage of blood samples were performed as described previously (49). Serum samples were measured for amplitude by chip-based sensing (see Fig. 5A). The rats were classified according to the threshold values determined (Fig. 5C-H) with amplitude > 0.800 as lean and < 0.760 as obese. s-HFD, vitamin-supplemented high-fat diet; HFD, normal high-fat diet; YGB, Roux-en-Y gastric bypass; VSG, vertical sleeve gastrectomy.

Surgery	Diet	Body weight		Amplitude	Classification	
		d 0	d 60		lean > 0.800	obese < 0.760
RYGB	s-HFD	513.13	463.50	0.826±0.092	x	
		469.77	480.40	0.841±0.083	x	
		448.56	419.90	0.853±0.101	x	
		541.54	594.10	0.734±0.067		x
		509.96	509.80	0.769±0.075	0	0
		513.37	465.10	0.819±0.070	x	
		423.14	431.60	0.833±0.059	x	
		481.76	427.40	0.809±0.049	x	
	HFD	407.72	445.60	0.812±0.051	x	
		507.79	468.60	0.803±0.060	x	
		513.78	477.00	0.795±0.058	0	0
		487.35	352.30	0.845±0.071	x	
		525.15	540.90	0.768±0.055	0	0
		382.72	359.99	0.821±0.071	x	
		550.42	531.50	0.755±0.040		x
		433.83	333.20	0.866±0.059	x	
VSG	s-HFD	501.80	464.70	0.839±0.049	x	
		500.60	537.60	0.733±0.038		x
		507.00	494.70	0.829±0.044	x	
		483.80	454.60	0.840±0.038	x	
		495.40	512.30	0.789±0.051	0	0
		472.50	521.30	0.797±0.045	0	0
		459.30	518.70	0.809±0.039	x	
	HFD	446.50	478.40	0.818±0.035	x	
		543.00	556.20	0.766±0.059	0	0
		555.11	567.30	0.737±0.044		x
		487.89	510.60	0.825±0.050	x	
		454.40	514.20	0.779±0.043	0	0
		463.70	454.10	0.836±0.039	x	
		468.00	470.00	0.827±0.045	x	
RYGB-sham	s-HFD	478.53	570.60	0.851±0.039	x	
		464.35	550.80	0.780±0.048	0	0
		539.32	677.00	0.707±0.052		x
VSG-sham	s-HFD	475.44	535.30	0.743±0.035		x
		452.70	566.40	0.818±0.040	x	
		511.50	633.50	0.759±0.057		x
		554.00	683.10	0.701±0.035		x
		478.30	608.20	0.725±0.041		x
RYGB-sham	HFD	427.93	491.40	0.798±0.050	0	0
		454.13	568.50	0.767±0.046	0	0
		485.25	582.90	0.741±0.030		x
		485.64	603.60	0.711±0.031		x
VSG-sham	HFD	524.30	574.20	0.720±0.029		x
		525.80	674.20	0.693±0.025		x
		481.36	534.70	0.753±0.037		x
		477.60	555.40	0.782±0.040	0	0

Comments: Consistent differences in amplitude as well as body weight between the type of bariatric surgery (RYGB, VSG) were not recognized. This indicates that the body weight loss *per se* was responsible for the surgery-induced increases in amplitude, which in most cases enabled classification of the individual rats as lean or obese using threshold values.

Supplemental Table S5. *Effect of cholesterol-extracting agents on amplitude reduction and phase shift elicited by serum complexes.*

Legend: Pooled serum samples from eight rats each were exposed (60 min, 4°C) to five different agents, which bind or sequester cholesterol when embedded in phospholipid mono- or bilayers, such as streptolysin-O (4.5 units/ml; SLO), digitonin (0.25 mg/ml; DIG), saponin (0.12 mg/ml; SAP), filipin (0.35 mg/ml; FIL) or nystatin (0.1 mg/ml; NYS) and buffer (Control) and then assayed for their effect on phase shift and amplitude. The experiments were performed (see Fig. 5) and are given as means ± SD of relative phase shift (PS) and amplitude reduction (AR) elicited by the complexes with control incubations set at 100 for each serum. * $p \leq 0.05$ *vs*. control.

Rat Serum	Control	SLO	DIG	SAP	FIL	NYS
lean ZF	AR=100±19	7± 3*	11± 4*	4± 3*	93±13	106±19
	PS=100±16	21± 6*	14± 6*	32± 9*	87±16	97±12
lean ZDF	AR=100±22	39±12*	10± 5*	73±14	96±28	90±13
	PS=100±25	4± 3*	41± 9*	28± 5*	103±11	88±22
obese ZF	AR=100±19	27± 8*	55±10*	82±21	95±19	115±17
obese ZDF	PS=100±15	45± 9*	20± 7*	70±11	83±15	76±12
lean Wistar	AR=100±20	59±13*	67±14*	48±14*	18±10*	24± 9*
obese Wistar	AR=100±18	79±17	71±12*	55±18*	29±16*	39±15*

Outcome: The five cholesterol-extracting agents caused decreases in phase shift and amplitude reduction with varying efficacy dependent on the serum and agent used: Streptolysin-O, digitonin and saponin efficient with lean Z(D)F rats, obese Z(D)F rats, lean Wistar and obese Wistar rats in that declining ranking order; filipin and nystatin highly potent with Wistar rats but inactive with Z(D)F rats. Thus, incubation of sera with cholesterol-extracting agents prior to measurement provoked significant declines in phase shift and amplitude reduction, which were dependent on the genotype and bodyweight of the rats and the type of agent.

Conclusion: These data are compatible with (i) cholesterol being a constituent of the rat complexes of GPI-AP and lipids, (ii) rat complexes being heterogenous with regard to their cholesterol content and physicochemical properties, which determine their differential susceptibility towards cholesterol extraction as well as their correlation to the metabolic state and (iii) differential extraction of cholesterol representing a useful criterion for the refined differentiation of metabolic states of rats.

Supplemental Table S6. *Patient characteristics and synopsis of the PIG37-dependent differences in phase shift and amplitude.*

Legend: Blood glucose, HbA1c levels and body weight of control and diabetic (T1D, T2D) probands (A-K) were measured. Determination of the SAW phase shift and amplitude with the fresh unfrozen serum samples was performed as described (Supplemental Figure S16). The differences in PIG37-dependent phase shift (Δ PS) and amplitude (Δ A) were calculated (see Δ in S16) and classified into mild (one arrow), moderate (two arrows) and considerable (three arrows), which reflect increase (↑), decrease (↓) or no change (↑↓) in phase shift and amplitude in response to injection of PIG37.

Proband	Age (years)	Gender	HbA1c (%)	Body Weight	State	Δ PS	Δ A
A	47	M	normal	lean	contr.	↓↓↓	↑↑↑
G	29	F	normal	lean	contr.	↓↓	↑↑↑
B	50	F	normal	lean	contr.	↓	↑↑
H	29	F	normal	lean	contr.	↓	↑
E	42	M	normal	lean	contr.	↑↑	↓↓
D	64	F	5.9	overweight	T1D	↑↓	↑↓
I	68	M	6.6	overweight	T2D	↓↓	↓↓
F	49	F	7.1	obese	T2D	↑↑	↑↓
C	41	F	5.5	obese	T1D	↓↓↓	↓↓↓
K	51	F	7.5	obese	T1D	↑↑	↓

Comments: Four out of five normal probands (A, G, B, H) displayed increases in amplitude and comcomitantly decreases in phase shift as expected for chip-based sensing of typical unprocessed serum GPI-AP in complex with lipids in the presence of PIG37. None of the patients with T1D or T2D shared this pattern, but rather exhibited decreases in both amplitude and phase shift (I, C) or no changes at all (D, F). One normal proband (E) and one patient (K) had in common decreases in amplitude and concomitantly increases in phase shift.

In conclusion, this preliminary investigation (small sample number, heterogenous disease phenotype) enabled the classification of four normal probands and four diabetic patients out of ten participants. This finding argues for the design of longitudinal studies with properly characterized and well defined healthy, prediabetic and diabetic participants of adequate number to evaluate the usefulness of chip-based sensing of unprocessed GPI-AP in serum for the prediction and stratification of metabolic diseases, such as diabetes.

Supplemental Table S7. *Comparative synopsis of relevant characteristics of the serum complexes between normal and hyperinsulinemic (hyperglycemic) rats.*

Legend: Phase shift and amplitude reduction were measured by chip-based sensing. The characteristics of the complexes of GPI-AP and lipids with regard to mass/size, release and viscosity/elasticity, which are compatible with the measured phase shift and amplitude reduction, the putative mechanisms of release and enzymic degradation of the complexes under consideration of the proposed cholesterol content in the lipid rafts and the predicted GPI-PLD activity in serum are given on the basis of the hypothetical model (see Supplemental Figure 18).

Rat	**Normal**	**Hyperinsulinemic (Hyperglycemic)**
Phase shift	**High**	**Low**
Spec. mass / size of serum complexes	**High**	**Low**
Release of complexes into serum	High	Low
Cholesterol in lipid rafts of releasing cells	High	Low
Amplitude reduction	**Low**	**High**
Viscosity / Elasticity of serum complexes	**Low / High**	**High / Low**
Degradation of the GPI-AP coat of complexes	Low	High
GPI-PLD activity in serum	Low	High

REFERENCES

67. **Müllner S**. Patent Application DOS DE 3623747 A1, 1986.

68. **Al-Awar A, Kupai K, Veszelka M, Szűcs G, Attieh Z, Murlasits Z, Török S, Pósa A, Varga C**. Experimental diabetes mellitus in different animal models. *Diabetes Res J* doi: 10.1155/2016/9051426, 2016.

69. **Miranville A, Herling AW, Biemer-Daub G, Voss MD**. Reversal of inflammation-induced impairment of glucose uptake in adipocytes by direct effect of CB1 antagonism on adipose tissue macrophages. *Obesity* 18: 2247-2254, 2010.

70. **Müller G, Jordan H, Petry S, Wetekam E-M, Schindler P**. Analysis of lipid metabolism in adipocytes using a fluorescent fatty acid derivative. I. Insulin stimulation of lipogenesis. *Biochim Biophys Acta* 1347: 23-39, 1997.

71. **Müller G, Schneider M, Gassenhuber J, Wied S**. Release of exosomes and microvesicles harbouring specific RNAs and glycosylphosphatidylinositol-anchored proteins from rat and human adipocytes is controlled by histone methylation. *Am J Mol Biol* 2: 187-209, 2012.

72. **Haldar K, Ferguson MAJ, Cross GAM**. Acylation of a Plasmodium falciparum merozoite surface antigen via sn-1,2-diacyl glycerol. *J Biol Chem* 260: 4969-4974, 1985.

73. **Müller G, Schubert K, Fiedler F, Bandlow W**. The cAMP-binding ectoprotein from Saccharomyces cerevisiae is membrane-anchored by glycosyl-phosphatidylinositol. *J Biol Chem* 267: 25337-25346, 1992.

74. **Müller G, Wetekam E-M, Jung C, Bandlow W**. Membrane association of lipoprotein lipase and a cAMP-binding ectoprotein in rat adipocytes. *Biochemistry* 33: 12149-12159, 1994.

75. **Fischer W, Ishizuka I, Landgraf HR, Herrmann J**. Glycerophosphoryl diglucosyl diglyceride, a new phosphoglycolipid from Streptococci. *Biochim Biophys Acta* 296: 527-545, 1973.

76. **Schneider P, Mc Conville MJ, Mehlert A, Homans SW, Bordier C**. Structure of the glycosyl-phosphatidylinositol membrane anchor of the Leishmania major promastigote surface protease. *J Biol Chem* 263: 16955-16964, 1990.

77. **Goldberg HA, Warner KJ**. The staining of acidic proteins on polyacrylamide gels: enhanced sensitivity and stability of "Stains-all" staining in combination with silver nitrate. *Anal Biochem* 251: 227-233, 1997.

78. **Howard SP, Buckley JT**. Membrane glycoprotein receptor and hole-forming properties of a cytolytic protein toxin. *Biochemistry* 21: 1662-1667, 1982.

79. **Gordon VM, Benz R, Fuji K, Lleppla SH, Tweten RK**. Clostridium septicum alpha-toxin is proteolytically activated by furin. *Infect Immun* 65: 4130-4134, 1997.

80. **Diep DB, Nelson KL, Raja SM, Pleshak EN, Buckley JT**. Glycosylphosphatidylinositol anchors of membrane glycoproteins are binding determinants for the channel-forming toxin aerolysin. *J Biol Chem* 273: 2355-2360, 1998.

81. **Abrami L, Fivaz M, van der Goot FG**. Adventures of a pore-forming toxin at the target cell surface. *Trends Microbiol* 8: 168-172, 2000.

82. **Diep DB, Nelson KL, Lawrence TS, Sellman BR, Tweten RK, Buckley JT**. Expression and properties of an aerolysin--Clostridium septicum alpha toxin hybrid protein. *Mol Microbiol* 31: 785-794, 1999.

83. **Shin D-J, Chuoy HE, Hong Y**. Use of Clostridium septicum alpha toxins for isolation of various glycosylphosphatidylinositol-deficient cells. *J Microbiol* 43: 266-271, 2005.

84. **Shin D-J, Lee JJ, Choy HE, Hong Y**. Generation and characterization of Clostridium septicum alpha toxin mutants and their use in diagnosing paroxysmal nocturnal hemoglobinuria. *Biochem Biophys Res Commun* 324: 753-760, 2004.
85. **Brodsky RA, Mukhina GL, Nelson KL, Lawrence TS, Jones RJ, Buckley JT**. Resistance of paroxysmal nocturnal hemoglobinuria cells to the glycosylphosphatidylinositol-binding toxin aerolysin. *Blood* 93: 1749-1756, 1999.
86. **Nelson KL, Raja SM, Buckley JT**. The glycosylphosphatidylinositol-anchored surface glycoprotein Thy-1 is a receptor for the channel-forming toxin aerolysin. *J Biol Chem* 272: 12170-12174, 1997.
87. **Rossjohn J, Buckley JT, Hazes B, Murzin AG, Read RJ, Parker MW**. Aerolysin and pertussis toxin share a common receptor-binding domain. *EMBO J* 16: 3426-3434, 1997.
88. **Zhao P, Nairn AV, Hester S, Moremen KW, O'Regan RM, Oprea G, Wells L, Pierce M, Abbott KL**. Proteomic identification of glycosylphosphatidylinositol anchor-dependent membrane proteins elevated in breast carcinoma. *J Biol Chem* 287: 25230-25240, 2012.
89. **Lim JM, Wollaston-Hayden EE, Teo CF, Hausman D, Wells L**. Quantitative secretome and glycome of primary human adipocytes during insulin resistance. *Clin Proteomics* 11(1):20. doi: 10.1186/1559-0275-11-20. eCollection, 2014.
90. **Brockman D, Chen X**. Proteomics in the characterization of adipose dysfunction in obesity. *Adipocyte* 1: 25-37, 2012.
91. **Rosenow A, Noben JP, Bouwman FG, Mariman EC, Renes J**. Hypoxia-mimetic effects in the secretome of human preadipocytes and adipocytes. *Biochim Biophys Acta* 1834: 2761-2771, 2013.
92. **Müller G, Wied S, Dearey E-A, Biemer-Daub G**. Glycosylphosphatidylinositol-anchored proteins coordinate lipolysis inhibition between large and small adipocytes. *Metabolism* 60: 1021-1037, 2011.
93. **Müller G, Dearey E-A, Korndörfer A, Bandlow A**. Stimulation of a glycosyl-phosphatidylinositol-specific phospholipase by insulin and the sulfonylurea, glimepiride, in rat adipocytes depends on increased glucose transport. *J Cell Biol* 126: 1267-1276, 1994.
94. **Müller G**. Let's shift lipid burden--from large to small adipocytes. *Eur J Pharmacol* 656: 1-4, 2011.
95. **Cieślak M, Roszek K**. Purinergic signaling in the pancreas and the therapeutic potential of ecto-nucleotidases in diabetes. *Acta Biochim Pol* 61: 655-662, 2014.
96. **Dzeja P, Terzic A**. Adenylate kinase and AMP signaling networks: metabolic monitoring, signal communication and body energy sensing. *Int J Mol Sci* 10: 1729-1772, 2009.
97. **Antonioli L, Blandizzi C, Csóka B, Pacher P, Haskó G**. Adenosine signalling in diabetes mellitus--pathophysiology and therapeutic considerations. *Nat Rev Endocrinol* 11: 228-241, 2015.
98. **Müller G, Jung C, Biemer-Daub G, Frick W**. Transfer of the glycosylphosphatidylinositol-anchored 5'-nucleotidase CD73 from adiposomes into rat adipocytes stimulates lipid synthesis. *Br J Pharmacol* 160: 878-891, 2010.
99. **Le Lay S, Krief S, Farnier C, Lefrere I, Le Liepvre X, Bazin R, Ferre P, Dugail I**. Cholesterol, a cell size-dependent signal that regulates glucose metabolism and gene expression in adipocytes. *J Biol Chem* 276: 16904-16910, 2001.
100. **Dagher G, Donne N, Klein C, Ferre P, Dugail I.** HDL-mediated cholesterol uptake and targeting to lipid droplets in adipocytes. *J Lipid Res* 44: 1811-1820, 2003.
101. **Dugail I, Le Lay S, Varret M, Le Liepvre X, Dagher G, Ferre P**. New insights into how adipocytes sense their triglyceride stores. Is cholesterol a signal? *Horm Metab Res* 35: 204-210, 2003.

102. **López-Cobo S, Campos-Silva C, Valés-Gómez M**. Glycosyl-Phosphatidyl-Inositol (GPI)-Anchors and Metalloproteases: Their Roles in the Regulation of Exosome Composition and NKG2D-Mediated Immune Recognition. *Front Cell Dev Biol* doi: 10.3389/fcell.2016.00097, 2016.
103. **Ilangumaran S, Robinson PJ, Hoessli DC**. Transfer of exogenous glycosylphos-phatidylinositol (GPI)-linked molecules to plasma membranes. *Trends Cell Biol* 6: 163-167, 1996.
104. **Kooyman DL, Byrne GW, McClellan S, Nielsen D, Tone M, Waldmann H, Coffman TM, McCurry KR, Platt JL, Logan JS.** In vivo transfer of GPI-linked complement restriction factors from erythrocytes to the endothelium. *Science* 269: 89-92, 1995.
105. **Anderson SM, Yu G, Giattina M, Miller JL**. Intercellular transfer of a glycosylphosphatidylinositol (GPI)-linked protein: release and uptake of CD4-GPI from recombinant adeno-associated virus-transduced HeLa cells. *Proc Natl Acad Sci USA* 93: 5894-5898, 1996.
106. **Müller G, Wied S, Jung C, Over S**. Hydrogen peroxide-induced translocation of glycolipid-anchored (c)AMP-hydrolases to lipid droplets mediates inhibition of lipolysis in rat adipocytes. *Br J Pharmacol* 154: 910-913, 2008.
107. **Müller G, Jung C, Wied S, Biemer-Daub G**. Induced translocation of glycosylphosphatidylinositol-anchored proteins from lipid droplets to adiposomes in rat adipocytes. *Br J Pharmacol* 158: 749-770, 2009.
108. **Ahmed KA, Xiang J.** Mechanisms of cellular communication through intercellular protein transfer. *J Cell Mol Med* 15: 1458-1473, 2011.
109. **Anderson C**. The end of theory. The data deluge makes the scientific method obsolete. *Science* 06.23.08, 2015.

DETAILED PROTOCOLS - Additional Experimental Details for Figs. 2-9

Fig. 2. Implementation of chip-based sensing of unprocessed GPI-AP.

(A) For capture of rat adipocyte EV, decreasing volumes of EV in EV buffer as indicated and adjusted to 200 µl final injection volume, which had remained untreated (turquoise and red curves) or had been pretreated with PI-PLC (black line) or had been depleted for GPI-AP (green curve), were sequentially injected into α-toxin-coated channels (turquoise, black and green curves) or RSA (red curve) or into "blank" uncoated channels (see below; period A). Phase shift is measured at a flow rate of 50 µl/min using EV buffer as running buffer and with regeneration after each injection (period B) and given (as °) upon correction for the "blank" channel and normalization (set at 0 for 250 sec; see Supplemental Figure S1A). Representative diagram from four independent coating reactions is shown performed with distinct chips.

(B) For "sandwich" detection of rat adipocyte EV by annexin-V and anti-CD73 antibodies, 162.5 µl of EV in EV buffer, which had been depleted for GPI-AP (period A) or left untreated (period B), were injected (at a flow rate of 13 µl/min) consecutively into α-toxin coated channels with (blue curve). For detection of unspecific binding of EV to serum albumin, 162.5 µl of 1% RSA in EV buffer were injected to yield the "albumin" channel by mere (non-covalent) adsorption (red curve). In addition, uncoated channels were run as "blank" channels. Subsequently, 162.5 µl each of 200 nM anti-caveolin antibodies (period C), 200 nM anti-CD73 antibodies (period D), 400 nM annexin-V containing 0.2 mM EGTA (period E) and 400 nM annexin-V containing 40 µM Ca^{2+} (period F) were injected successively into the channels. Phase shift is measured at a flow rate of 13 µl/min using EV buffer as running buffer and given (as °) upon correction for the "blank" channel (see A) and normalization (set at 0 for 0 sec). Representative diagram from five independent detection reactions is shown performed with three distinct chips and two distinct samples.

Comment: A considerable phase shift was observed with RSA in the presence of annexin-V and Ca^{2+}. Since albumin is a major component of serum and cell media, an "albumin" channel with RSA (in PBS) injected was included in the following experiments for correction of α-toxin-independent binding of annexin-V to the chip (possibly caused by its interaction with phospholipids associated with chip surface-adhering albumin from the serum or medium samples.

(C) For studying the concentration-dependence of the "sandwich" detection of captured EV by annexin-V, 75 µl of EV in EV buffer were injected into α-toxin-coated channels or into a "blank" channel. Subsequently, 2x130 µl of annexin-V at the concentrations indicated in EV buffer containing 40 µM Ca^{2+} (period A) and then 2x130 µl of EV buffer as running buffer (period B) were injected into the channels at a flow rate of 30 µl/min. Phase shift is given (as °) upon correction for the "blank" channel and normalization (set at 0 for 0 sec and each annexin-V concentration) as both original and fitted data. Representative diagram from three independent detection reactions is shown performed with five distinct chips and the same sample.

(D) For studying the volume-dependence of capture and detection of adipocyte EV, increasing volumes of EV in EV buffer, adjusted to a total sample volume of 2x130 µl each, were injected into α-toxin-coated channels or into a "blank" channel. Subsequently, 2x130 µl of 400 nM annexin-V and 40 µM Ca^{2+} in EV buffer were injected into all channels (period A), followed by injection of EV buffer as running buffer at a flow rate of 30 µl/min (period B). Phase shift is given (as °) after correction for the “blank” channel and normalization (set at 0 for 0 sec and each volume performed with six distinct chips and two distinct samples).

(E) For studying the effect of PIG37 on capture of EV, 150 µl of EV in EV buffer in the absence (black curve) or presence of PIG37 at the concentrations indicated (red, green, pink, blue curves) were injected into α-

toxin-coated channels or into a "black" channel at a flow rate of 20 µl/min (period A). Subsequently, 225 µl of EV buffer containing 200 µM PIG37 or lacking PIG37 was injected at a flow rate of 20 µl/min (period B). Phase shift is given (as °) upon correction for the "blank" channel and normalization (set at 0 for 0 sec and 200 µM PIG37; blue curve) as original and fitted data. Representative diagram from two independent detection reactions is shown performed with two distinct chips and two distinct samples.

(F) For detection of unprocessed GPI-AP in adipocyte incubation medium, increasing volumes of medium obtained by incubation of rat adipocytes of medium size and kept untreated (black, red, green curves) or depleted for GPI-AP (dark blue curve) or pretreated with PI-PLC (light blue curve) or nitrous acid (NA; pink curve) or medium lacking adipocytes (control; violet curve) and adjusted to 150 µl total volume with adipocyte buffer each were injected into α-toxin-coated channels. Subsequently, 2x150 µl of 20 mM TRIS/HCl (pH 8.0), 150 mM NaCl, 250 mM sucrose containing 400 nM annexin-V and 40 µM Ca^{2+} were injected at a flow rate of 25 µl/min (period A). Thereafter, 1 ml of 20 mM TRIS/HCl (pH 8.0), 150 mM NaCl and 250 mM sucrose were injected at a flow rate of 75 µl/min (period B). Phase shift is given (as °) upon correction for the "blank" channels and normalization (set at 0 for 0 sec and 150 µl volume) as original and fitted data. Representative diagram from three independent detection reactions is shown with the same chip and two distinct (medium) samples.

Fig. 3. Implementation of chip-based sensing of plasma membrane-derived GPI-AP using the "lab-on-the-chip" configuration.

For immobilization of plasma membranes from small (A) or large (B) adipocytes, three 100-µl portions in 10 mM HEPES/KOH (pH 7.5), 150 mM NaCl and 100 mM sucrose (PM) in the presence of 2 mM EGTA (light green curve) or 1 mM Ca^{2+} (blue curve) and, alternatively, three 100-µl portions of running buffer were consecutively injected into α-toxin-coated channels or uncoated "blank" channel (red curve) at a flow rate of 20 µl/min at 20°C (period A). For demonstration of the presence of the insulin receptor α-chain (IRα), 100 µl of 25 nM anti-IRα antibodies were injected at the end of period A. For the putative generation of unprocessed GPI-AP from the immobilized plasma membranes and their capture by the α-toxin-coated chip, 24 ml of running buffer containing 30 µM PIG37 were injected at a flow rate of 200 µl/min at 37°C (period B). For release of the plasma membranes from the chip surface, 1 ml of 10 mM glycine (pH 10) containing 2 mM EGTA were injected at a flow rate of 100 µl/min, followed by injection of 300 µl of running buffer alone (blue and red curves) or buffer containing 0.05% BATC (black curve), 1.5% BATC (pink curve), PLA_2 (green curve), 200 µM PIG41 (turquoise curve) or 100 mM mannose (yellow curve) at a flow rate of 100 µl/min at 20°C (period C). For demonstration of capture of unprocessed GPI-AP, 200 µl of 400 nM annexin-V, 40 µM Ca^{2+}, 10 mM HEPES/KOH (pH 7.5), 150 mM NaCl and 100 mM sucrose, 150 µl of running buffer, 180 µl of 200 nM anti-CD73 antibodies, 10 mM HEPES/KOH (pH 7.5), 150 mM NaCl and 100 mM sucrose, 90 µl of running buffer, 90 µl of 25 nM anti-IRα antibodies, 10 mM HEPES/KOH (pH 7.5), 100 mM sucrose, 150 mM NaCl and 0.2 mM EGTA, 65 µl of running buffer, 130 µl of 200 µM PIG41, 10 mM HEPES/KOH (pH 7.5), 100 mM sucrose, 150 mM NaCl and 0.2 mM EGTA and finally 90 µl of 10 mM HEPES/KOH (pH 7.5), 150 mM NaCl and 100 mM mannose were injected at a flow rate of 13 µl/min at 20°C in that sequential fashion (period D). Phase shift (as °) is given upon normalization (set at 0 for 0 sec). Representative overlay diagrams from six independent runs for each condition (periods A-D) are shown performed with three distinct chips (and the channels re-used six times), the same samples and the same instrument. The calculation of the specific GPI-AP-induced phase shift as the difference between the total (normalized) phase shift after

binding "in sandwich" of both annexin and anti-CD73 antibodies with subsequent washings (at 14500 sec) and the unspecific phase shift left after injection of PIG41 (1500 sec) is indicated.

Comments: Successful immobilization of negatively charged liposomes was reported previously, but interpreted as the formation of flat tethered phospholipid bilayers rather than of (sealed) vesicles on the chip surface (25, 26). At present, this possibility can not be excluded for the immobilized adipocyte plasma membranes. The differential sensing of the unprocessed GPI-AP for small *vs*. large adipocytes was considerably impaired by omission of PIG37 during the simultaneous release and capture of the unprocessed GPI-AP (period B, data not shown).

Fig. 4. Effect of flow rate and adipocyte size on generation of complexes from plasma membranes.

Plasma membranes from small (blue and pink curves) or large (green and turquoise curves) adipocytes were injected into α-toxin-coated channels or "blank" channels lacking a protein coat (not shown) in the presence of 1 mM Ca^{2+} for immobilization (see Figure 2; period A). Unprocessed GPI-AP were generated from the immobilized plasma membranes by injection of running buffer containing 30 µM PIG37 at a flow rate of either 200 µl/min (green and blue curves) or 25 µl/min (pink and turquoise curves)(period B, not shown). The plasma membranes were detached from the chip surface by the injection of glycine (pH 10) containing EGTA and subsequently of running buffer (period C, not shown). Captured GPI-AP were detected by consecutive injections of annexin-V in the presence of Ca^{2+}, anti-CD73 antibodies and anti-IRα antibodies with intervening washings with running buffer and finally by injection of PIG41 and mannose (period D). The phase shifts (A**,** as °) and amplitudes (B, as arbitrary units) measured during period D are given upon correction by subtracting the values of the "blank" channel and normalization (set at 0 and 1, respectively, for 7200 sec). Representative overlay diagrams from four independent experiments (periods A-D, D shown only) for each adipocyte size and flow rate with the same chip (after regeneration) are shown performed with the same samples. The calculation of the specific phase shift (A) or amplitude reduction (B) induced by unprocessed GPI-AP as the differences between the total (corrected and normalized) signal after injection "in sandwich" of annexin-V and anti-CD73 antibodies with subsequent washings (10900 sec) and the unspecific signal remaining after injection of PIG41 (11400 sec) is given.

Comments: Phase shift as well as amplitude reduction turned out to be positively correlated to the flow rate of the buffer streaming through the microfluidic chip channels for both small and large adipocytes. These findings suggest that the size of the plasma membrane donor adipocytes and the velocity of the passing extracellular fluid are positively correlated to the amount, spec. mass / size and viscosity of the complexes of unprocessed GPI-AP and phospholipids which are released from plasma membranes in the lab-on-the-chip.

Fig. 5. Chip-based sensing of unprocessed GPI-AP from rat serum.

(A) For PIG37-dependent differentiation between obese Wistar, ZF and ZDF rats upon simultaneous capture and detection of GPI-AP, 40 µl of pooled serum sample from obese Wistar (black curve), ZF (turquoise curve) and ZDF (red curve) rats diluted five-fold with PBS and incubated (10 min, 20°C) with 200 µl of 800 nM annexin-V and 80 µM Ca^{2+} were injected into α-toxin-coated channels at a flow rate of 120 µl/min and at 20°C (period A1). To initiate the differentiation, 100 µl of 30 µM PIG37 in PBS were injected at a flow rate of 20 µl/min and at 37°C (period B1). To regenerate the chips, 50 µl of 200 µM PIG41 in PBS were injected at a flow rate of 15 µl/min for displacement of unprocessed GPI-AP (period C1), followed by injection of 2x150 µl of PBS containing 0.2 mM EGTA and 0.05% NP-40 at a flow rate of 90 µl/min for removal of phospholipids

(period D1) and finally of 2x100 µl of PBS at a flow rate of 90 µl/min (period E1). To demonstrate reproducibility of this protocol, the periods A-D were repeated under identical conditions with slightly adapted time frames. Phase shift (upper panel) and amplitude (lower panel) are given (in ° and arb. unit, respectively) after correction for the "blank" and "albumin" channels and normalization (set at 0° and 1 arb. unit, respectively, for start of the injection at 0 sec) as original data. The maximal phase shift and minimal amplitude, respectively, measured after the injection of PIG37 at the end of period B are indicated as hatched lines. The differences in maximal phase shift and minimal amplitude between obese Wistar and ZDF rats are indicated (red Δ), obese Wistar and ZF rats (turquoise Δ) and obese ZDF and ZF rats (black Δ) as measured at the end of period B1/2 (presence of PIG37) with Δ representing increases and -Δ decreases. Representative diagram from six independent runs for each serum type is shown performed with two distinct chips (re-used four times) and the same samples.

(B) The differences (absolute values) in phase shift [°] and amplitude [arb. units] between obese Wistar and ZDF (red bars), obese Wistar and ZF (turquoise bars) and obese ZDF and ZF (black bars) rats measured at the end of period A1/2 (absence of PIG37) or period B1/2 (presence of PIG37) are given as means $\pm$ SD (* $p \leq 0.05$; $^{\#}$ $p \leq 0.01$) calculated from four independent runs for each serum type performed with four distinct chips (re-used six times) and the same samples and instrument. In the following experiments the phase shift and amplitude were measured at the end of period B.

(C-H) For the comparative analysis of serum GPI-AP from rats of similar body weight and different genotype, phase shift (C, D, G) and amplitude (E, F, H) were measured in the presence of 30 µM PIG37 as described for (A) are given for the individual samples and the means M $\pm$ SD calculated thereof as well as the pooled samples P $\pm$ SD derived from 12 (M) and 4 (P) independent runs for each sample performed with one chip (re-used six times) and 12/4 setting for each rat group ($^{\#}$ $p \leq 0.05$, * $p \leq 0.01$).

Comments: The pooled serum samples (P) from eight individual measurements for the lean ZDF (C) and ZF (E) rats exhibited significantly reduced phase shifts (C) and amplitudes (E), respectively, compared to those of lean Wistar rats. Importantly, each individual lean ZDF and ZF rat displayed a phase shift (C) and amplitude (E), respectively, below the means - 1xSD (M) of lean Wistar rats (green curves) and, *vice versa*, seven and eight, respectively, out of eight individual lean Wistar rats (brown and blue curves) above the mean + 1xSD of lean ZDF (C) and ZF (E) rats, respectively. The pooled serum samples (P) from the eight individual measurements for the obese ZDF (D) and ZF (F) rats demonstrated significantly lower phase shifts (D) and amplitudes (F), respectively, compared to those of obese Wistar rats. Similar differences were also observed for the calculated means of the corresponding individual samples (M). Importantly, for each individual obese ZDF (red line) and six out of seven individual obese ZF (red line) rats displayed phase shifts (D) and amplitudes (F), respectively, below the means - 1xSD (M) of obese Wistar rats. *Vice versa*, seven out of eight (yellow line) and each (pink line) individual obese Wistar rats displayed phase shifts (D) and amplitudes (F), respectively, above the means + 1xSD (M) of obese ZDF (D, yellow line) and ZF (F, pink line) rats. Albeit both phase shift (G) and amplitude (H) were significantly lower for obese ZDF compared to ZF rats on basis of the pooled serum samples (P), the calculated means (M) represented trends, only. Nevertheless, six and seven obese ZDF rats (pink lines) were below the mean - 1xSD for the phase shift (G) and amplitude (H), respectively, of obese ZF rats and *vice versa* five and six out of seven obese ZF rats (yellow lines) were above the mean + 1xSD (M) for phase shift (G, yellow line) and amplitude (H, yellow line), respectively, of obese ZDF rats. Taken together, differentiation between individual obese ZDF and ZF rats is possible on basis of (trends between) the corresponding means of phase shift as well as amplitude.

Fig. 7. Effect of physical treatments of unprocessed GPI-AP on their differentiation potential.

The differences in the maximal phase shift and minimal amplitude between obese Wistar and ZDF rats and between obese Wistar and ZF rats, respectively, were measured (see Fig. 5A) and are given as mean ± SD from four or eight independent treatments for each sample with measurements performed in duplicate with the channels re-used up to six times.

(A) Effect of sample processing and storage. Serum samples were thawed at 37°C and then subjected to the indicated numbers of freezing and thawing cycles in either "rapid" mode (freezing in liquid N_2 and thawing at 37°C) or "slow" mode (freezing at -20°C and thawing at 20°C) or "routine" mode (single cycle of freezing at -20°C and thawing at 37°C) before measurement. * $p \leq 0.05$ and $^{\#}$ $p \leq 0.01$ *vs*. R.

(B) The effect of temperature. Serum samples were thawed (37°C) and then incubated (60 min) at the temperatures indicated before measurement or measured immediately after thawing (Control). * $p \leq 0.05$ and $^{\#}$ $p \leq 0.01$ *vs*. Control.

(C) Effect of mechanical forces. Serum samples were thawed (37°C) and then centrifuged using the conditions indicated or the "routine" mode (R, 1000x*g* for 5 min, as performed with the rat serum samples). The supernatants were removed and immediately measured. * $p \leq 0.05$ and $^{\#}$ $p \leq 0.01$ *vs*. R. (D) Effect of ultrasonic waves. Serum samples were thawed (37°C) and then subjected to cycles of ultrasonic treatment (5-sec bursts at 80 W and 35 kHz with 10-sec intervals at 4°C; Bandelin electronic RF 100) before measurement or measured immediately as control (C). * $p \leq 0.05$ and $^{\#}$ $p \leq 0.01$ *vs*. C.

(E) Effect of vibration. Serum samples were thawed (37°C) and then subjected to the indicated numbers of vibration cycles (10-sec treatments at max. speed with 10-sec intervals each; neoLab Vortex Mixer 7-2020) before measurement or measured immediately as control (C). * $p \leq 0.05$ and $^{\#}$ $p \leq 0.01$ *vs*. C.

(F) Putative similarities between unprocessed GPI-AP from different sources were investigated. Serum from obese ZDF rats, incubation medium of primary rat adipocytes of large size and purified EV from large rat adipocytes were tested for their susceptibility towards physical treatments (see A-E) in comparison. Phase shift and amplitude reduction (see Supplemental Figure S3A) are given as means ± SD from two independent experiments for each sample and measurements in duplicate with the corresponding control treatments (identical incubation temperature and period without treatment) set at 100%.

Fig. 8. Characterization of unprocessed GPI-AP derived from rat adipocyte plasma membranes (A, B) or present in human serum (C, D).

(A, B) The experiment was performed with plasma membranes from small (blue, green, pink curves) and large (yellow, brown, turquoise curves) adipocytes as described for Fig. 3, however, using a flow rate of 200 µl/min during period B (3000-10200 sec). At the end of period B, the chips were removed from the instrument without emptying of the channels and put into sealed and fitted plastic chambers. Chips with captured GPI-AP from small or large adipocytes were exposed to ten cycles of vibration (20-sec treatments at max. speed with 20-sec intervals each; neoLab Vortex Mixer 7-2020; pink, brown lines) or three cycles of ultrasound treatment (2-sec bursts at 80 W and 35 kHz with 20-sec intervals at 4°C; Bandelin electronic RF 100; yellow and turquoise lines). Other chips were left untreated as controls (green, blue curves). Phase shift (A, as °) and amplitude (B, as arbitrary units) were measured during period D and corrected by subtracting the values of the "blank" channel and normalization (set at 0 and 1, respectively, for 10800 sec). Representative overlay diagrams from four independent runs for each condition and adipocyte size (period D shown only) are shown

performed with the same chip (and channels re-used four times) for each adipocyte size with two distinct chips each.

(C, D) 40 µl of pooled serum sample from normal probands A and B)(C) and diabetic patients C and D)(D) diluted five-fold with PBS was injected into α-toxin-coated or "blank" channels at a flow rate of 60 µl/min and at 20°C using running buffer (period A0). Prior to the injection, the samples were kept untreated (Control) or incubated (2 h, 30°C) with PC-PLC from *Chlostridium perfringens* (10.0 mU/ml) or with EGTA (2 mM) or with PLA_2 from honey bee venom (2.5 mU/ml), 0.02% BSA, 144 mM NaCl, 2 mM Ca^{2+}, 0.5 mM DTT and 0.2 mM PMSF or with α-toxin-coupled microspheres (subsequent centrifugation; see Methods) or with PIG41 (200 µM) or with BATC (1%) and 144 mM NaCl or with PI-PLC (0.25 mUml) from *Bacillus cereus* or with human GPI-PLD (0.075 mU/ml) or with HF or with NA (see online methods). To demonstrate stable capture of unprocessed GPI-AP by the chip, 240 µl of running buffer were injected subsequently into the channels at a flow rate of 120 µl/min and 37°C. Thereafter, 270 µl of 400 nM annexin-V containing 40 µM Ca^{2+} were injected at a flow rate of 90 µl/min (period A1). To demonstrate stable detection of unprocessed GPI-AP by the chip, 240 µl of running buffer were injected subsequently into the channels at a flow rate of 120 µl/min and 37°C. Thereafter, 52 µl of 200 nM anti-CD73 antibodies were injected at a flow rate of 26 µl/min and 37°C (period B). To demonstrate stable detection of GPI-AP "in sandwich", 400 µl of running buffer were injected subsequently into the channels at a flow rate of 120 µl/min and 37°C. Phase shift (C, as °) and amplitude (D, as arbitrary units) are given upon correction for the "blank" and "albumin" channels and normalization (set at 0 for start of the injection at 0 sec after the pretreatments) as original data. Representative overlay diagrams from two independent pretreatments of the same serum samples and three independent measurements using distinct chips are shown.

Fig. 9. PIG37-dependent sensing of unprocessed GPI-AP in serum of control subjects and diabetic patients.

40 µl of pooled serum sample diluted five-fold with PBS were injected into α-toxin-coated or "blank" channels at a flow rate of 80 µl/min and at 20°C using running buffer (period A0). Following washing by injection of 170 µl of running buffer at a flow rate of 200 µl/min and 37°C, 280 µl of 400 nM annexin-V containing 40 µM Ca^{2+} were injected at a flow rate of 120 µl/min (period A1). Subsequently, the channels were rinsed with 230 µl of running buffer at a flow rate of 200 µl/min and 37°C, followed by injection of 130 µl of 30 µM PIG37 at a flow rate of 30 µl/min (period B) and then of 230 µl of running buffer at a flow rate of 200 µl/min. Regeneration of the chips was accomplished by sequential injection of 180 µl of 200 µM PIG41 at a flow rate of 60 µl/min and 37°C (period C), then of 200 µl of running buffer at a flow rate of 200 µl/min and finally of 900 µl of running buffer containing 0.2 mM EGTA and 0.05% NP-40 at a flow rate of 200 µl/min (period D). Phase shift (as °) and amplitude (as arb. u.) are given upon correction for the "blank" and "albumin" channels and normalization (set at 0° and 1 arb. unit, respectively, for start of the injection at 0 sec) as original data. Representative overlay diagrams from three independent measurements (as indicated by distinct colors) using distinct channels of the same chip are shown. The maximal phase shifts and minimal amplitudes, respectively, measured at the end of the consecutive injection of annexin-V + Ca^{2+} (period A1) and PIG37 (period B) are indicated as hatched lines. These PIG37-dependent changes in phase shift and amplitude are marked by triangles for each serum sample. Δ / - Δ indicates increase / decrease of phase shift or amplitude in comparison to the absence of PIG37 (i.e. difference between end of period B and A1). A, Control person; I and F, overweight and obese T2D patients, respectively.